January 2013

Exploring The Differences In Deep Convective Transport Characteristics Between Quasi-Isolated Strong Convection And Mesoscale Convective Systems Using Seasonal Wrf Simulations

Brandon Clifford Bigelbach

Follow this and additional works at: https://commons.und.edu/theses

EXPLORING THE DIFFERENCES IN DEEP CONVECTIVE TRANSPORT
CHARACTERISTICS BETWEEN QUASI-ISOLATED STRONG CONVECTION
AND MESOSCALE CONVECTIVE SYSTEMS USING SEASONAL WRF
SIMULATIONS

by

Brandon Clifford Bigelbach
Bachelor of Science, St. Cloud State University, 2010

A Thesis
Submitted to the Graduate Faculty

of the

University of North Dakota

in partial fulfillment of the requirements

for the degree of

Master of Science

Grand Forks, North Dakota
August
2013

This thesis, submitted by Brandon Clifford Bigelbach, in partial fulfillment of the requirements for the Degree of Master of Science from the University of North Dakota, has been read by the Faculty Advisory Committee under whom the work has been done and is hereby approved.

_____
Gretchen Mullendore

_____
Mark Askelson

_____
Leon Osborne

This thesis is being submitted by the appointed advisory committee as having met all of the requirements of the School of Graduate Studies at the University of North Dakota and is hereby approved.

_____
Wayne Swisher
Dean of the School of Graduate Studies

_____
Date

PERMISSION

Title	Exploring the differences in deep convective transport characteristics between quasi-isolated strong convection and mesoscale convective systems using seasonal WRF simulations
Department	Atmospheric Sciences
Degree	Master of Science

In presenting this thesis in partial fulfillment of the requirements for a graduate degree from the University of North Dakota, I agree that the library of this University shall make it freely available for inspection. I further agree that permission for extensive copying for scholarly purposes may be granted by the professor who supervised my thesis work or, in her absence, by the Chairperson of the department or the dean of the School of Graduate Studies. It is understood that any copying or publication or other use of this thesis or part thereof for financial gain shall not be allowed without my written permission. It is also understood that due recognition shall be given to me and to the University of North Dakota in any scholarly use which may be made of any material in my thesis.

<div style="text-align: right">

Brandon Clifford Bigelbach
July 18, 2013

</div>

TABLE OF CONTENTS

LIST OF FIGURES

LIST OF TABLES

ACKNOWLEDGEMENTS

First and foremost, I must acknowledge my advisor, Dr. Gretchen Mullendore, for taking in a scared new graduate of St. Cloud State University and turning him into a confident scientist. You pushed me when I needed it and even when I did not so that I kept moving forward, culminating in this M.S. degree. You have never given up on me, and in such have helped me never give up on myself, and I am so very thankful for that. Allowing me to be a part of your group and help lead the group has been such an enriching experience. Also, having the confidence in me to be your first Ph. D. student truly humbles me. I must also acknowledge all of the hard work, time, and effort that was put forth in helping me get to this degree by the rest of my advising committee: Dr. Mark Askelson and Leon Osborne. Your interest in my work and in helping me with this study has been invaluable, and I sincerely thank you both.

Secondly, I must thank my family and closest friends for the care, love, and support they have shown for me, being near to some and very far from others. My wife, Michelle deserves the most thanks for being there always, and being so open and flexible living with a graduate student, and all that it entails. Even when I did not want to do something, or was unsure of something that I was doing, you always push me to go for it, no matter what, and follow my dream. I am forever grateful for all that you do for me, and for all that we do together. I would like acknowledge my

immediate family: My parents Carla and Mike, my brother Benjamin, my in-laws Michael Roskos Sr., Janet Roskos, and Michael Roskos Jr. Also my closest friends: Michael Stanga, Jason Bednar, Nicole Blomgren, Michael Hollan. To the other members of my research group, I thank you for all the helpful advice I have received on my project. To all of my fellow graduate students and to my undergraduate friends here at the University of North Dakota, thank you for all that you have done for me to support me and help me through these last three years, and for all the support to come.

ABSTRACT

It has been shown in several previous studies that there is a relationship between mesoscale storm type and deep convective mass transport characteristics. For example, a previous simulation study showed that a supercell storm transported significantly more tracers into the stratosphere than did a multicell storm in an environment with identical thermodynamic structure. We utilize the Weather Research and Forecasting (WRF) model (version 3.2.1) with chemistry to simulate mass transport during the convective season of 2007 in the U.S. Southern Great Plains at convection-resolving scale (2 km). The storms that were resolved in the model were then classified using an object-based classification scheme. This classification scheme, which is based on schemes used in the mesoscale observational community, uses model-derived radar reflectivity (a function of precipitation hydrometeors) to classify storm type as either weak convection, quasi-isolated strong convection (QISC), mesoscale convective system (MCS), or linear MCS.

This study focuses on examining the differences between the QISC and MCS regimes. Differences on the domain-scale are determined by investigation of two transport parameters: the level of maximum detrainment (LMD) and the magnitude of newly transport mass. Based on total transport over the entire region, results have shown that there are some significant differences between regimes. The LMD is significantly higher in the MCS regime than in the QISC regime in July, but the LMD is very similar in the two regimes in May. Conversely, the magnitude of newly transported mass in the

MCS and QISC is very similar in July, but significantly different in May. At a *per storm* scale, differences were determined by analysis of the magnitude of transport per deeply convective object and the LMD relative to the height of the tropopause. The tropopause-relative LMD followed the domain-wide results, where there were significant differences in July but the regimes transported to similar altitudes in May. There were significant differences in the magnitude of transport per deeply convective object for both May and July.

CHAPTER I

INTRODUCTION

Upward vertical transport of chemical constituents via deep convection is
important to the chemical makeup of the troposphere and lower stratosphere, and has
profound implications on air quality and climate (e.g. Dickerson et al., 1987; Barth et al.
2007). Dickerson et al. (1987) assert that deep convective transport can turn a local
pollution problem into a global problem, as the residence times of transported chemicals
are much greater in the stratosphere than in the planetary boundary layer (PBL). The
importance of convection to the transport of chemical constituents has been
acknowledged in many studies (e.g. Hintsa et al. 1998; Mullendore et al. 2005; Lawrence
and Salzmann 2008; Sigmond et al. 2010). Although it is not the only mechanism by
which boundary layer constituents are transported to the upper-troposphere-lower-
stratosphere (UTLS) region, it is certainly the most rapid of the mechanisms.

Previous studies of resolved deep convective transport have focused on either
individual cases or individual storm regimes (e.g., Thompson et al. 1994; Stenchikov et
al. 1996; Barth et al. 2007; Halland et al. 2009). Additionally, many of these studies
(e.g., Pickering et al. 1992; Hintsa et al. 1998) have found variance in their data, which
may be attributable to variance in storm regimes. This study builds on those studies and
on that of Mullendore et al. (2005), who found that both an idealized and a real supercell
produced more transport to the stratosphere than an idealized multi-cellular storm.

However, to date, there has been no systematic study of deep convective transport differences between isolated strong convection (including both milticell and supercell storms) and mesoscale convective systems (MCSs). The goal of this study is to utilize an objective classification scheme for determining dominant storm regimes and to determine which regime, isolated strong convection or MCS, is the most efficient at transporting air from the PBL to the UTLS region. By utilizing completely passive tracers in the Weather Research and Forecasting with Chemistry (WRF-CHEM) model, the altitude of deep convective mass transport and the magnitude of that transport are determined for each of the simulated storms and are averaged over the domain. Further per-storm analysis is performed to identify features that are important to individual storms for each regime.

CHAPTER II

BACKGROUND

Deep convection efficiently transports mass from the planetary boundary layer

(PBL) to the upper troposphere and lower stratosphere (UTLS) region and is a very

important component of the global budget of chemical constituents in the atmosphere.

Deep convective transport is the focus of this project: it is important, however, to

understand the many different pathways by which mass is transported. The primary

mechanism by which mass is transported in the atmosphere is large-scale motion

(Lawrence and Salzmann 2008), with large-scale upward motion in the tropics and large-

scale downward motion at the poles. In the extratropics, synoptic scale disturbances,

such as mid-latitude cyclones, redistribute mass in the vertical over a period of days.

Note that similar redistribution, although over a smaller horizontal scale, occurs in

convection on an hourly timescale (Sigmond et al. 2000; Mullendore et al. 2005).

Focusing on exchange between the troposphere and stratosphere, Holton et al. (1995)

found that tropospheric air is transported to the stratosphere primarily in the tropical

latitudes by the Brewer-Dobson circulation. In the extratropics, Hintsa et al. (1998)

described three methods by which mass is transported to the lowermost stratosphere (the

area between the local tropopause and the tropical tropopause, assumed to be at 380 K);

these three methods are diabatic descent from the overworld ($\theta > 380$ K), isentropic

transport across the tropopause in regions of tropopause folds, and deep convection.

Convection transports the smallest amount of mass of these three methods, but is the

fastest, and can also transport undiluted boundary layer air to the UTLS region, which

can have important chemical outcomes, as described later in this chapter.

In order to study the scientific question of the study, which is to determine the

differences in transport characteristics between isolated strong convection and MCSs, it is

important to understand previous work performed in the following areas: primary tracer

species in convective transport, simulating deep convection and convective transport, and

thunderstorms classification. Primary tracer species in convective transport have been

considered in previous studies in which simulations of transport of chemical constituents

(mainly carbon monoxide and ozone) from the PBL to the UTLS region were performed.

It is important, in attempt to aid in the determination of the model setup for the current

study, to know how previous studies chose to model the atmosphere for studies of general

convection and for transport by deep convection, and these studies are discussed in the

simulating deep convection and convective transport section. Finally, an important

component of this study is thunderstorm classification. Thus, previous relevant studies

that utilized thunderstorm classification are considered.

Use of Tracers in Deep Convective Transport Studies

The best way to track transport of air in thunderstorms is through the use of

tracers. Tracers can be either actual chemical constituents or they can be completely

passive species (similar to food coloring in water). Numerical models that include

chemical processes can initiate and advect both passive tracers and chemical constituents

in simulations. When studying deep convective transport, it is beneficial to use chemical tracers that are passive on the time scale of convection (i.e. less than 12 hours). Two such chemical tracers, carbon monoxide (CO) and ozone (O_3) have been used as proxies for boundary layer air and stratospheric air, respectively, in many deep convective transport observational and modeling studies (e.g. Dickerson et al. 1987). However, as described below, urban areas may also have significant O_3 concentrations in the boundary layer. Additionally, many studies have used non-chemical tracers in models that do not predict chemical processes to study storm processes (e.g. Mullendore et al. 2005). Results from these studies using passive tracers can be extrapolated to the "real world" by relating passive tracers to species that have relatively large reaction times, such as CO.

CO has been both measured and modeled as a tracer in many transport studies, including Scala et al. (1990), Pickering et al. (1992), Thompson et al. (1994), Poulida et al. (1996), Stenchikov et al. (1996), Fischer et al. (2003) Hegglin et al. (2004), Barth et al. (2007), and Halland et al. (2009). CO is an ideal tracer of deep cumulus convective transport because it is nearly insoluble in the presence of H_2O, it is rapidly detected with sensors, and its concentration generally decreases with altitude (Dickerson et al., 1987). Near surface concentrations of CO in the United States are estimated to be typically >200 ppbv in urban areas, 100-200 ppbv in rural areas, and <100 ppbv in remote areas (e.g., Jacob, 1999).

Cotton et al. (1995) estimated that the mass of air in the planetary boundary layer (PBL) is vented, or transported out of the PBL, about 90 times in a calendar year due to clouds and cloud systems. It has been found that only a small amount of the overall PBL airmass is transported directly to the upper troposphere, since the PBL is subject to

mixing and modification before vertical transport takes place (Scala et al., 1990).

Thompson et al. (1994) estimated that about half of the PBL air is vented to the free troposphere by deep convection in the early summer months, and that CO transport out of the PBL to the free troposphere was about 18.1×10^8 kg per month for the month of June. They also determined that upward deep convective flux is the largest term in the budget of PBL CO.

As stated above, venting of the PBL by deep convection does not necessarily deposit PBL air into the upper troposphere and lower stratosphere. Halland et al. (2009) state that air in the updraft disperses from the cloud in via detrainment along three paths: 1) through the core of the updraft, 2) by traversing the anvil of the storm or, 3) along cloud edges. Mullendore et al. (2005) asserted that air transported to a specific altitude remains there, i.e. is irreversibly transported, only if the parcel is neutrally buoyant at that level due to heating processes. The possible heating processes they discussed were latent heating and turbulent mixing with warmer environmental air (in the lower stratosphere). Detrainment (and entrainment) of air can take place in many different levels of the storm, as shown in Fig. 1 Cohen et al. (2000). In that study, six different cumulonimbus clouds were simulated and entrainment and detrainment properties were analyzed for each. Figure 1 shows an example of local maxima of detrainment for one cloud (dashed lines around 12.5 km, 8.5 km, and between 2-5 km).
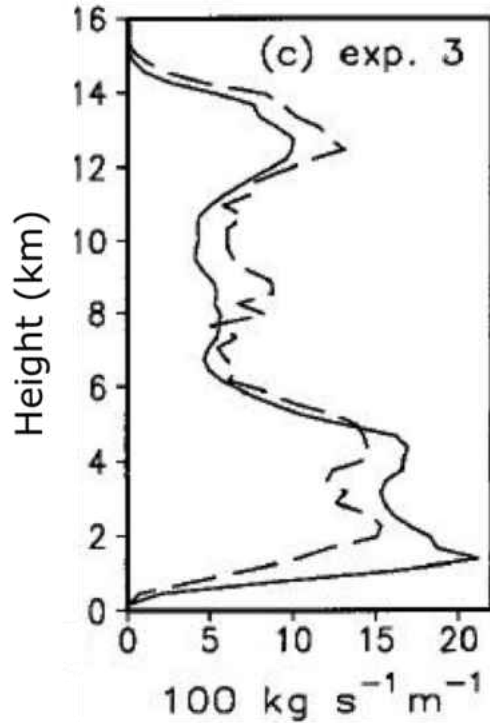
Fig. 1. Updraft entrainment rates (solid lines) and detrainment rates (dashed lines) for one of six simulated cumulonimbus clouds. Figure 12 from Cohen et al. (2000).

Mullendore et al. (2009) defined the level of maximum detrainment (LMD) to be the altitude at which the maximum amount of mass is detrained out of a storm. They identified the LMD using the vertical velocity divergence profile. For a storm that occurred on 26 January 1999 during the Tropical Rainfall Measuring Large-Scale Biosphere-Atmosphere (TRMM-LBA) campaign, they found the minimum of the total vertical divergence (the LMD) to be at approximately 11.25 km, which agreed with the estimated LMD altitude that was estimated using radar reflectivity structure in the anvil.

Using the LMD provides a better calculation of detrainment at the top of the storm in the upper troposphere/lower stratosphere region as compared to detrainment estimated by using the level of neutral buoyancy (LNB) calculated from parcel theory because it accounts for storm-scale dynamics such as vertical pressure gradients (which

affect parcel speed and the height to which parcels can be transported) and entrainment of environmental air into a storm (Mullendore et al. 2013). These levels were compared for multicell storms, supercell storms, and convective lines by Mullendore et al. (2013). Using LMD and LNB altitudes, the found that supercells transported mass higher relative to the LNB than did multicell storms and convective lines. This result agrees with Mullendore et al. (2005), who identified more transport to the stratosphere in a simulated supercell than in a simulated multicell that developed in an environment having the same amount of convective available potential energy (CAPE).

Beyond acting as a quasi-passive tracer, CO is also important as it is a precursor to ozone (O_3) in the troposphere. The majority of O_3 precursors are emitted close to surface (Fischer et al., 2003). Pickering et al. (1992) found that O_3 production in urban plumes was greater than in clean air, and also that injection of precursors (like CO) may enhance O_3 production by factors of 2-50 or even more. They concluded that urban areas that are subject to frequent deep convection may significantly add to mid-tropospheric amounts of O_3 and its precursors on a regional and perhaps global scale, which in turn significantly impacts regional chemistry.

In the stratosphere, O_3 absorbs the ultra-violet rays from the sun (Park et al. 2001), protecting human and animal skin from its harmful effects. It is also efficient at absorbing long-wave radiation. Therefore, in the upper troposphere, the main role of O_3 is as a greenhouse gas (e.g. Pickering et al. 1992; Hegglin et al. 2004; Halland et al. 2009). In summary, CO and other trace species transported from the boundary layer have a significant impact on the creation and depletion of O_3, which in turn has profound effects on the radiation budget of the atmosphere.

Simulating Deep Convection and Convective Transport

a) Model Sensitivities

Determining a model set-up that realistically simulates the atmosphere being studied requires running case studies using different combinations of parameterizations to determine sensitivities. Presented herein are results of studies that focused on sensitivities to different parameterizations, varied spin-up times (i.e., the time the model is "spinning up" to a more realistic atmospheric state, prior to any analysis), and model resolution. Model resolution is very important to determining what scales of motion are resolved. This subsection also provides a summary of the most popular physics parameterization choices available with the Weather Research and Forecasting (WRF; Skamarock et al. 2008) model.

Many possible WRF-model configurations exist, and any changes in configuration impact the solution. Spin-up time and physical parameterizations are just two of the ways one can edit the model configuration. Weisman et al. (2008) and Aligo et al. (2009) both utilized WRF version 2.0 (Weisman et al. 2008 also utilized version 1.3) and showed that convective systems and precipitation regimes were reasonably reproduced after 3-5 hours of spin-up time utilizing model grid spacing of 4 km. Anything in the first 3-5 hours is subject to error in spinning up the model dynamics and physics due to a "cold start" of the WRF model, which means that no direct data assimilation is utilized and no convective systems exist at initialization time. This is also consistent with the work of Skamarock (2004), who found that small-scale structures were effectively spun up in the initial 6-12 hours of their simulations.

Physical parameterizations are another major factor that can drastically affect model solutions. Processes that occur on the sub-grid scale and thus are not explicitly resolvable must be parameterized. Such processes include radiation, cumulus convection, cloud microphysics, and eddy mixing in the PBL. Much work has been done with sensitivity testing of certain parameterizations.

Weisman et al. (2008) performed an array of convective simulations using WRF versions 1.3 and 2.0.3.1 with different physics parameterization configurations. One of the parameterizations that was tested was the PBL scheme, and of those schemes that were tested, one of importance was the Mellor-Yamada-Janjić (MYJ) PBL scheme (Janjić 2001). The MYJ scheme builds the PBL via mixing between model levels based upon turbulent kinetic energy (TKE) calculations. The length scale for eddies is determined from the combination of TKE and the buoyancy and shear profiles. The MYJ scheme solves for TKE production and dissipation iteratively. Kain et al. (2005), using WRF version 2.0, found that the MYJ scheme tends to deepen the PBL slowly, which results in characteristics of the PBL that are cooler, more moist, and more capped than other schemes. Further, it has been found that the specification of the land surface characteristics, especially soil moisture, is, at times, critical to adequate representation of the evolution of the PBL (Trier et al. 2004). Trier et al. (2004) also stated that land surface characteristics can be critical to the representation of initiation and evolution of convection. Other examples of PBL schemes include the Yonsei University scheme (Hong et al. 2006) and the Quasi-Normal Scale Elimination (QNSE) scheme (Sukoriansky et al. 2006). The YSU scheme features determination of the PBL top via the buoyancy profiles, or, specifically, where the critical bulk Richardson number is

equal to 0. It also features a countergradient term to determine unstable PBL fluxes and it explicitly handles entrainment at the PBL top. The QNSE scheme features partial averaging of features, which allows for consideration of different grid resolutions, amongst other parameters. It also differs in that it contains a nonzero value of the eddy viscosity when the Richardson number is less than or equal to 1, when most schemes tend the viscosity term to zero. It also analyzes the effects of internal wave generation in the presence of turbulence.

Microphysical parameterizations also strongly affect evolution of simulated convective storms. These schemes include adjustment of the saturation at the end of each time step to account for the updated temperature and moisture fields (Skamarock et al., 2008). They also predict size distributions of hydrometeors and number concentrations of species as well. A double moment scheme allows for the size distribution for hydrometeors to vary. A comparative study of single and double-moment microphysics schemes were performed on an atmospheric river event by Jankov et al. (2010), using WRF version 3.0. They found that the Thompson microphysics scheme (Thompson et al., 2004), along with others, performed well with reproducing high clouds, but struggled with mid-level clouds and overestimated clear-sky conditions. The Thompson scheme features a variable gamma distribution for cloud droplets, lookup tables for freezing droplets and the transition of cloud ice to snow, and variable collection efficiencies for rain, snow, and graupel that collect cloud droplets. Weisman et al. (2008) tested the Thompson scheme on a squall line case for their study and found that it was able to reproduce that squall line as the other microphysics schemes used, although they note the convective core seemed reduced in size and the stratiform region more extensive.

Morrison et al. (2009) compared performance of a one-moment and two-moment microphysics scheme in WRF version 2.2, based upon the work of Morrison and Pinto (2005) and Morrison et al. (2005), when simulating a trailing stratiform region of a squall line. They found that the two-moment scheme produced a more extensive trailing stratiform region and a sharper precipitation gradient between the convective and stratiform regions. The Morrison et al. (2005) scheme features a user switch for hail/graupel, prediction of the mixing ratio and number concentration of four phases of water (rain, snow, graupel, cloud ice) and mixing ratios of cloud droplets and vapor, and gamma distribution size parameters determined by these predicted values. Two of the many other schemes used in WRF are the Lin et al. (1983) scheme, and the WRF double-moment six class scheme (WDM6). The Lin scheme features an exponential Marshall-Palmer size distribution (Marshall and Palmer 1948) for rain, snow, and graupel. It determines hail growth via probabilistic freezing of raindrops and uses autoconversion for the collection-coalescence and collection-aggregation efficiencies. The WDM6 scheme features the same mixing ratio and number concentration predictions that the Morrison scheme calculates. This scheme features mixed phase fall speeds for snow and graupel that are determined by assignment of a single fall speed to both and weighing each by its predicted mixing ratio.

Also important is the convective parameterization. This parameterization is utilized in simulations with coarse resolutions (on the order of approx. 10 km or greater in the horizontal) to effectively release latent heating due to convection and vertically mix the atmosphere (Skamarock et al., 2008). In a study of an East coast cyclone, Mahoney and Lackmann (2006) compared results from the operational Eta that employed

the Betts-Miller-Janjić (BMJ;Betts and Miller, 1993; Janjić, 1994) and the Kain-Fritsch schemes (KF; Kain and Fritsch, 1993). They found that the BMJ produced low pressure centers associated with a distinct local convective maximum with a weak coastal front. In contrast, the KF produced more uniform convective precipitation associated with a uniform inverted trough signature and a stronger coastal front. They admitted, for their case in question, that overall the KF scheme produced more realistic results than the BMJ scheme. In contrast, other tests of sensitivity to convective parameterizations indicated that the BMJ scheme is somewhat comparable to the KF scheme. Jankov et al. (2005) found that the BMJ scheme increased areal coverage of light rainfall and lowered system total rainfall, as compared to the KF scheme. However, microphysical parameterizations were changed at the same time, making it unclear whether the changes in precipitation and coverage were due to the convective scheme, microphysics scheme, or the interaction of both. Gallus et al. (2005) studied an MCS and derecho event and compared results from different models (WRF, Eta, and MM5) that utilized both the KF and BMJ schemes. They found that the Eta-BMJ and the WRF-BMJ simulations produced the least amount of error in the position of the MCS. All models had major displacement errors with the KF shceme, as did the MM5-BMJ simulation.

Model resolution is also a significant factor that impacts model solutions. As years have progressed, and computational power has increased, so has the ability to perform simulations at higher resolutions while keeping the computation time roughly the same. A coarse resolution simulation, where Δx and Δy is greater than 10 km, for example, may have profound solution differences from that of a fine resolution run, where Δx and Δy are less than or equal to O(1 km) (Weisman et al., 1997). A rule of

thumb exists for deep convection that the grid spacing required to resolve convection is O(1 km) (Wilhelmson and Wicker, 2001). This grid spacing would resolve a typical thunderstorm that has approximate horizontal dimensions of 10 km. However, Bryan et al. (2003) state that this rule of thumb can actually be inadequate in some situations. In one of their runs, they produced convection that had a scale of 4-6 km, which is a roughly the minimum that 1 km grid spacing can resolve. When they performed simulations with a gridspacing of 125 m, they could resolve convective circulations on a 1-2 km scale. Bryan et al. (2003) suggested that grid spacing of 1 km may not be sufficient to effectively resolve finer-scale attributes of storms, such as entrainment and convective overturning, and concluded that the only way to simulate, with any accuracy, the inertial subrange, is to perform model runs with horizontal resolution of O(100 m).

Other studies such as Bélair and Mailhot (2001), Clark et al. (2007), and Weisman et al. (2008) have acknowledged that model resolution is an important factor to accuracy. Weisman et al. (2008) found that parameterized convection simulated with the 12 km operational Eta model reproduced some of the qualitative features of the simulated storms. However, the timing of the system and the size of some of the convective features were not accurate. In the case studied, it was found that the slowness of system development was primarily due to errors in the simulated cold pool, which formed and strengthened too slowly. Clark et al. (2007) found that a convective parameterization on a 22-km grid had persistent problems forming coherent propagating rainfall and produced some areas of precipitation entirely too early, when compared to results produced using 5-km grid spacing. Bélair and Mailhot (2001) found that, for a squall line, fine-resolution runs with grid spacing of 2 km resolved the convective and anvil precipitation regions

14

fairly well, but that results were worse as grid spacing became coarser. They found that, for 18-km grid spacing, the intensity of precipitation was greatest in the anvil region, and that the precipitation in the convective region was not reasonably represented.

b) Parameterized transport

Although this study utilizes resolved convection for determining convective transport, it is also important to discuss how convective transport is handled at the parameterized scale, because findings at resolved scales can be used to discern possible errors in parameterized transport. Convective transport at the parameterized scale is widely used because it is significantly more computationally efficient than simulating at the resolved scale, and for certain studies, such as global chemical transport, resolved convective transport is computationally infeasible. The WRF model includes parameterized transport through the mass flux schemes available in the convective parameterization schemes, and by coupling the chemistry with these flux calculations. Some studies, in which convection is not explicitly resolved (e.g., Lelieveld and Crutzen 1994; Mahowald et al. 1997b; Collins et al. 1999; Lawrence et al. 2003b; Doherty et al. 2005) have determined that simulating transport with no convective parameterization can lead to drastic under-representation of transport. Lawrence and Salzmann (2008) highlighted the importance of transport via convective parameterizations, in which they stated that the parameterization allows for transport to occur as rapid, episodic vertical transport cells, as is the case in transport via the updraft.

Convection, in atmospheric models, can be either explicitly represented or parameterized. When parameterizing convection is necessary, there are two main types of schemes that one can employ: convective adjustment and mass-flux. A convective

adjustment scheme adjusts a convectively unstable environment to a prescribed state which is usually a sounding profile. For the mass-flux schemes, once convection is triggered, explicit calculations of profiles of cumulus mass fluxes and thermodynamic variables are performed each time step until closure has been reached. Two examples of mass-flux parameterization schemes available in the WRF model, BMJ and KF, were already introduced in the model sensitivity section above. Transport of trace gases in models with parameterized convection is handled by the mass flux calculations as well as by advection calculated in the model dynamics. It is of note that transport of tracers only occur in mass flux schemes, and as such mass flux schemes will be the focus of the rest of this section.

Transport schemes can have varying degrees of closure, from quasi-diffusive to bulk-entrainment (e.g., Mahowald et al. 1995). It has been found that the biggest differences between different mass-flux schemes for trace gasses are in the simulated vertical distributions of the gasses (Zhang et al. 2008). They concluded that the difference in vertical distributions between schemes highlight the uncertainty associated with the different formulations of the parameterizations. These differences in mass-flux formulations will be explained in more detail in the following subsections.

1) Parameterization process

The first step in the parameterization process is the trigger function. This is a criterion that determines when to initiate convection, thereby parameterizing the physical processes that dictate convective initiation and that are not all well understood (Bechtold et al. 2001). This can be formulated in different ways. Tiedtke et al. (1989) formulated their trigger function with a virtual temperature condition. If the virtual temperature of

16

an air parcel originating from the surface at a given level plus 0.5 K was greater than the

virtual temperature of the environment, that layer was said to be unstable. The trigger

function of the Bechtold et al. (2001) scheme is more complex. A 60 hPa mixed layer is

constructed at the surface where the trigger function is calculated. The basis for the

formulation is similar to Tiedtke et al. (1989); however, the Bechtold et al. (2001)

scheme uses virtual potential temperature as opposed to virtual temperature for

determining if a layer above the LCL is stable or unstable, as given by

$$\bar{\theta}_v^{mix} - \bar{\theta}_v + \Delta T / \Pi > 0, \tag{1}$$

where $\bar{\theta}_v$ is the mean virtual potential temperature, the superscript *mix* means that the

mixed-layer originating parcel is used, ΔT is the temperature change in a given layer ,

and the Exner function, Π, is given by:

$$\Pi = \left(P / P_{00} \right)^{R_d / C_{pd}}. \tag{2}$$

where P is the pressure at the top of the layer, P_{00} is the reference pressure, R_d is the gas

constant for dry air, and C_{pd} is the specific heat at a constant pressure for dry air. The

third term of (1) represents the change of potential temperature over the layer. Meeting

the condition of (1) means that the layer is considered to be unstable. If a layer is found

to be stable, then the function is calculated for the next layer of 60 hPa, and so on.

The next step in the parameterization process is the adjustment stage, in which the

modeled atmosphere works back to quasi-equilibrium. Arakawa (2004) describes this

step as the production of negative feedback to destabilization. This is also the step in

which the rate at which chemical species are transported through the model column is

determined, which is commonly deemed as the mass flux. Tracer mass fluxes are

strongly dependent on the difference in the entrainment and detrainment rates as calculated by a parameterization (Tiedtke et al. 1989; Langner et al. 1990; Bechtold et al. 2001).

In the Tiedtke et al. (1989) scheme, the entrainment of mass into the cloud occurs through both turbulent mixing of mass through the cloud edges and through organized inflow associated with larger scale convergence. Detrainment occurs through turbulent mixing and through outflow at cloud top. Both conditions for entrainment are considered only in the lower levels of the cloud, as turbulent mixing is only important in the lower levels for this scheme since it is much stronger there than at higher levels. Large-scale convergence, which is proportional to moisture convergence, is only considered where it is normally encountered, which is below the area of maximum vertical velocities.

Bechtold et al. (2001) describes their entrainment and detrainment rates as being inversely proportional to cloud radii, and are calculated by taking the product of the mass flux in the transition zone between clear and cloudy air (which is a function of the updraft mass flux times some parameters that include the inverse of cloud radius) and the fractional entrainment rates as defined by Kain and Fritsch (1990). Langner et al. (1990) prescribed entrainment and detrainment rates for their mass flux calculations based upon latitude and the season. They used the entrainment rates that were used were determined by Olofsson (1988), and the detrainment rates that were determined by Chatfield and Crutzen (1984).

The final step to forming transport parameterization schemes is closure, which means that the environment has been adjusted back to a non-convective (closed) state. Arakawa (2004) defines parameterizing convection as "the problem of formulating the

statistical effects of moist convection to obtain a closed system for predicting weather and climate." Closure for numerical models, then, can be said to be way in which the parameterized processes are related to the large-scale motions (see the right half of Fig. 2). At the top of Figure 2 is the control. This refers to the large-scale processes that help to de-stabilize the atmosphere, or to initiate the adjustment process. Then the convection processes are carried out on the RHS of Figure 2. The feedback is the part of the process that brings the atmosphere back to quasi-equilibrium, or back to a non-convective state. The last step of the process, on the LHS of Figure 2, is the resolved processes, which include the heating and condensation of the atmosphere as a result of cumulus convection. Both Tiedtke et al. (1989) and Bechtold et al. (2001) provide descriptions of how closure is reached for their respective schemes, and these closures are described below.
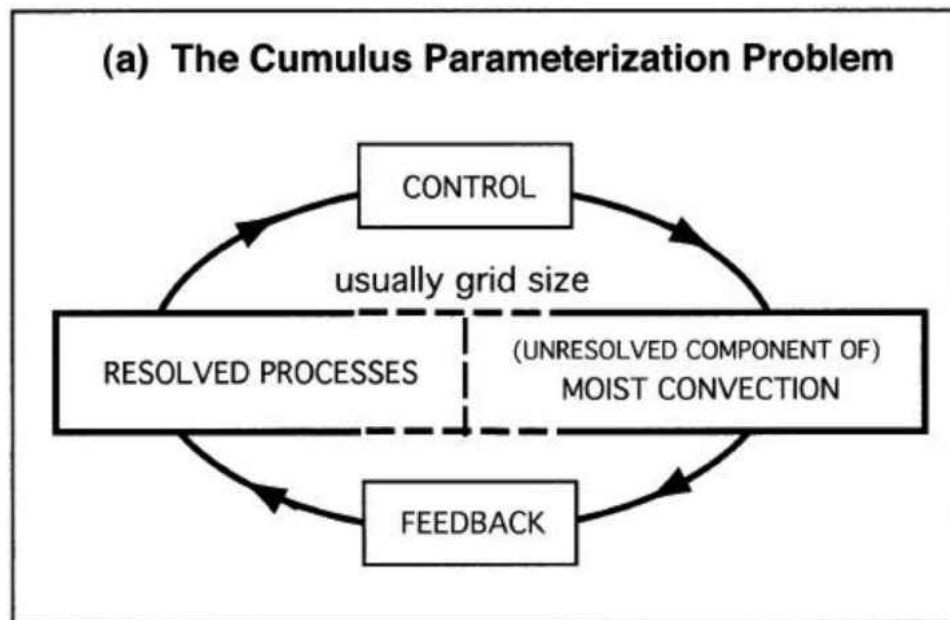
Fig. 2. The cumulus parameterization cycle, as taken from Arakawa et al. (2004).

The closure for the Tiedtke et al. (1989) scheme is based on moisture balance. In their scheme, mass fluxes are linked to large-scale and low-level moisture convergence. This makes sense as low-level convergence should lead to rising motion and if the column is moist, then clouds should form and moist convection would be the result. The scheme can be inferred to be considered closed when there is no longer any large-scale low-level moisture convergence, or it has fallen below a certain threshold in which there would no longer be any more cloud production.

The closure that is utilized in the Bechtold et al. (2001) scheme is based on convective available potential energy (CAPE). It is assumed that all CAPE in the grid is removed during adjustment to the non-convective state. The time for this removal is restricted to $0.5 < t < 1$ hr. They state that this is equivalent to the life cycle of one convective cloud. New values of thermodynamic variables are calculated, including CAPE, using an iterative procedure. After these quantities are calculated, they are multiplied by an adjustment factor dependent on the initial value of CAPE and the calculated value of CAPE for each time step. The process is repeated until the final CAPE is one tenth of the original value. Once that threshold is reached, the final environmental convective tendencies are evaluated.

2) Parameterization comparison

As stated above in the *Model Sensitivities* subsection, sensitivity testing is a very useful tool for evaluating differences between parameterizations. One study that investigated sensitivity of simulated mass transport to different model physics choices performed a variety of tests with seven cumulus parameterizations and two boundary layer parameterizations (Mahowald et al. 1995). Tests were performed to compare radon

profiles to that of Liu et al. (1984), compare the height of convection in models to that observed by the Central Equatorial Pacific Experiment, and to compare on-line and off-line mass fluxes. The data were averaged over three months for eight locations in the western U.S. Mahowald et al. (1995) found that, for midlatitude continental convection, the Tiedtke et al. (1989) scheme produced results that were closely matched to observations of radon, simulating, with the exception of the 1-3 km layer, concentrations within one standard deviation of observed values at all altitudes. The Tiedtke et al. (1989) scheme outperformed others used in their study. The measure of performance was determined by "scoring" how well each scheme reproduced the following items (including, but not limited to): radon quantity, the quality of the radon structure, and reproduction of depth of convection for two different field campaigns.

Another study that set out to compare different convective parameterization schemes (no tracer transport included) was performed by Tost et al. (2006). For their study, four parameterization schemes were used: the Tiedtke et al. (1989) scheme, the operational ECMWF model parameterization (Bechtold et al. 2004), the Zhang-McFarlane-Hack scheme (Zhang and McFarlane 1995; Hack 1994), and the Bechtold et al. (2001) scheme. The time domain for the study included 3 months of spin up time and 6 years of simulation for a general circulation model (GCM). Average precipitation was computed over the six-year period for precipitation and was compared to data collected in the Global Precipitation Climate Project (GPCP) and the Tropical Rainfall Measuring Mission (TRMM). Statistics (bias, root mean square error, and correlation) were calculated for several variables associated with the hydrologic cycle, as they state that accurate representation of the processes involved is crucial for radiative transfer

processes and atmospheric chemistry. All schemes overestimated precipitation amounts compared to observations. Also, differences between observed and modeled water vapor distributions were greatest near the UTLS region, especially in lower latitudes. This may be related to the simulated depth of the convection and precipitation formation efficiency. Overall, relative to observations no single scheme was considerably better than any other.

Tost et al. (2010) expanded upon the study of Mahowald et al. (1995). Five transport parameterizations were used in their study. The first was a modified version of the Tiedtke et al. (1989) scheme with the modification coming from Nordeng (1994). Also used was the Zhang-McFarlane-Hack scheme (Zhang and McFarlane 1995; Hack 1994) with a modification of the Zhang and McFarlane (1995) part of the scheme by Wilcox (2003). The other three schemes were the Bechtold et al. (2001) scheme, the ECMWF scheme (Bechtold et al. 2004), and the Emanuel and Zivkovic-Rothman (1999) scheme. The time domain for this study was 1 September 2005 to 1 January 2006, or four months. The meteorological variables were nudged towards ECMWF data.

For CO, use of different convective parameterizations lead to differences in modeled vertical profiles of +/- 20%. However, it must be noted that the concentration of OH (which CO reacts strongly with) that was modeled also affected the concentrations of CO. For ozone, the choice of parameterization had zonally averaged distribution differences of 5-25%. The complexity of the reactions and transport of ozone did not allow for an analysis of direct associations of distribution to either chemical or physical processes. They concluded that the choice of parameterization did have a significant effect on distributions of trace gases, with maximum differences of +/- 100%. These

differences arose from variability in both the meteorological and chemical processes between the different simulations.

It has been shown, through analysis of the previous studies, that there is no universally "best" transport parameterization. In Mahowald et al. (1995) it was clear that the Tiedtke et al. (1989) parameterization did a better job of reproducing profiles of radon and of simulating deep convection than did the other schemes. On the other hand, Tost et al. (2006) and Tost et al. (2010) found that there was no discernible difference in ability to consistently reproduce observations among the schemes that they tested. It is acknowledged that any study comparing different parameterizations may produce different results, depending on the meteorological situation that the study is using as its basis.

3) Implementation in numerical models

Some numerical models combine chemical processes and convective parameterization through offline chemical modeling. Grell et al. (2005) describe that in offline chemical modeling the chemistry and the meteorology are independent of each other in the model. Meteorological variables are prescribed in the chemical model from either reanalysis or separate, previous model runs. The transport and chemistry are driven by the meteorological data, which are usually made available every 30 to 60 minutes. They describe this method as computationally attractive as one meteorological dataset can yield many different chemistry simulations.

An offline chemical model that has been shown to reasonably represent the chemistry of the troposphere is the Model for Ozone and Related Chemical Tracers (MOZART, Emmons et al. 2010) model. This model is a global chemical transport

model (CTM) for the troposphere and stratosphere that can utilize a variety of meteorological datasets and emissions inventories.

Online chemical modeling is when the chemistry and the meteorology have two-way interaction, which allows for each to influence the other and provides for a more meteorologically realistic solution. An example of an online chemical model is WRF-CHEM, which is the base WRF model with a built-in chemistry package that allows the meteorology and the chemistry to interact online. Some of the chemical processes that can be simulated using WRF-CHEM include emissions (biogenic and anthropogenic), aerosols and their interactions, and passive tracer transport (Grell et al. 2005). Parameterized transport of chemistry in the WRF-CHEM model is handled by the mass flux part of the parameterization (see detailed description of mass flux parameterization in the prior section). One scheme available in WRF-CHEM was created by Grell (1993) and then expanded upon by Grell and Dévényi (2002). This scheme, as described by Grell and Dévényi (2002), is an ensemble scheme having 13,824 members. The individual members/perturbations arise from the three main parts of the scheme: the dynamic control, the feedback, and the static control (loosely related to the top, LHS, and RHS, respectively, of Fig. 2).

As described by Grell (1993), the dynamic control handles the modulation of the convection by the environment. This part of the scheme determines where and how strong the convection will be (the size is assumed to be fixed). The feedback is the modification of the environment by the convection. This part of the scheme determines how the temperature and moisture fields in the large-scale environment are changed as a result of advective and convective processes. Finally, the static control portion defines

the properties of the cloud. Such properties for the updraft and downdraft include, but are not limited to: entrainment and detrainment, cloud-base mass flux, updraft condensate, and evaporation of the condensate in the downdraft.

The three main assumptions used for closure in the dynamic control are based upon stability and moisture convergence, with two coming from the former and one from the latter. The first of the stability closures is the quasi-equilibrium assumption, in which the total available buoyant energy is in quasi-equilibrium between large-scale effects and that of cumulus convection. The second assumption is called the pure instantaneous stability closure. This assumption arises from the idea that the available buoyant energy due to cumulus convection is removed over a known time period. Finally, an assumption relates the amount of convective activity to the integrated vertical advection of moisture (Grell 1993, and references herein). This assumption is used in determining rainfall rate.

Sixteen different members are contained in the scheme's dynamic closure (Grell and Dévényi 2002). Each of these members are allowed to interact with each of the 22 individual members from the static control/feedback mechanisms. In the original implementation, each member was executed on each grid point. Once that was done, statistical analysis utilizing probability density functions was used to determine the most probable combination member. From there, a Bayesian formulation for determining the *a posteriori* density is used to determine the solution that is fed back into the model.

The way that WRF-CHEM implements this scheme is similar to the original implementation. The same assumptions are used in the model implementation. However, fewer perturbations are available for the ensemble, with a total 144 members. Also, none of the statistical methods for determining the most probable solution are used.

In the WRF-CHEM scheme, the solutions are merely averaged. This average value is then fed back into the model.

Classification of Thunderstorms

The main purpose of this research is to determine how transport characteristics vary with convective regime. Thunderstorms occur in a wide range of environments and exhibit a spectrum of different morphologies. Because different classification criteria are deemed important for different convective processes, there unfortunately exists no universally accepted classification scheme for convective regimes. Further, no previous studies have implemented a classification scheme solely for deep convective transport studies. However, a review of previously used classification schemes is useful for informing any new schemes that are developed, and to determine which approach will be used for classification herein.

Many recent studies have utilized storm regime classification to answer research questions. The classification of thunderstorms has been mainly subjectivelybased on radar reflectivity attributes (e.g. Bluestein and Jain, 1985; Weisman and Klemp, 1986; Parker and Johnson, 2000; Gallus et al., 2008; Schoen and Ashley, 2011). The main problem with classification of storm morphology is that it can be very subjective. In reality, storm structure covers a whole continuous spectrum of morphologies and also evolves over time, thereby not conforming to a single bin type classification scheme (e.g.,

Vasiloff et al., 1986; Parker and Johnson 2000; Done et al. 2004; Grams et al. 2006; Gallus et al., 2008).

The most basic classification scheme came from Weisman and Klemp (1986). They identified three classes--single cell, multi-cell, and supercell--defined by radar reflectivity characteristics. Bluestein and Jain (1985) classified four squall line types based on radar reflectivity. Nine classes of thunderstorm morphologies were also identified by Gallus et al. (2008).

Schoen and Ashley (2011) had four major storm classifications: unorganized cellular, organized cellular, quasi-organized cellular, and organized linear. Three of the four classes had sub-classifications, with unorganized cellular being the only one without. Their goal was to associate storm morphology to fatalities reported with storms. Instead of using predominant regime classification, they used a point classification approach in which the reflectivity field at the closest time to the storm report was used for classification. They acknowledged that many studies have used different classification approaches and that their definitions of storm morphologies were similar to those used in previous studies. They also stated that a universal classification system should be developed to improve post-event analyses.

Another study utilized more of an objective method to classify storms by using a decision tree (Gagne et al., 2009). They used their decision tree to classify storms into three classes: cellular, multi-cellular, and linear system. The cellular class has two sub-classes and the linear system class has three sub-classes based on the position of the stratiform region compared to the main convective region. They found that the decision trees had very strong classification skill and accuracy. They concluded that decision trees

that are trained using model reflectivity data could provide reliable storm classification in real time, and that trees trained using real world radar data could classify real storms with very little loss in accuracy.

Studies have used storm attributes other than reflectivity for classification. Moller et al. (1994) based a broad regime classification upon two attributes: buoyancy and wind shear. They asserted that unorganized convection had characteristically low buoyancy and weak winds, whereas organized convection exhibited high shear and strong winds. They discussed that unorganized storms are more "pulse-like" in nature with successive cells forming in more inconsistent manner mainly due to the complexity of outflow interactions. With increasing shear and instability, they stated that as the organization of the storms began to increase, new cells formed in more of a predictable location to its predecessor. They defined supercells differently, however. The criterion for a supercell that they provided was the existence of a mesocyclone, which has a vertical relative vorticity greater than or equal to 10^{-2} s^{-1} that persisted for a time scale of O(10 min) or greater and was present through at least one third of the convective storm depth. They concluded that through the use of the many tools available, such as storm relative helicity, radar reflectivity and radial velocity, the Bulk Richardson Number, Convective Available Potential Energy, and the classification method mentioned above, forecasters at the National Weather Service (NWS) should be able to detect supercells throughout its spectrum of morphologies and warn the public appropriately.

In summary, classifying thunderstorms is a difficult task. The spectrum of thunderstorm regimes is continuous, and classifying using rigidly delineated classes means risking not accounting for important information regarding storms. Schemes

discussed in the literature are based upon the requirements/needs of the individual

studies. For example, in studies such as Schoen and Ashley (2011), wherein the classes

described above were used, the focus was on hazardous weather and severe weather

reports. Gagne et al. (2009), on the other hand, used decision trees to identify classes for

the purpose of developing objective methods for classifying storms using simulated radar

reflectivity factor. It can be concluded that when approaching research that involves

classifying thunderstorms, the resulting scheme should be based upon the

requirements/needs of that individual study.

Dynamics of Quasi-Isolated Strong Convection and Mesoscale Convective Systems

The focus of the analysis herein is on the two strong regimes, quasi-isolated

strong convection (QISC) and mesoscale convective systems (MCS). This is due to the

two regimes being dynamically separate and important, both in terms of structure of the

storm and in terms of transport characteristics. The QISC regime consists of a few

different storm types (i.e., single-cell, multicell, and supercell convection). The

important features that make these two classes different is described here, with most of

the information discussed taken from Markowski and Richardson (2010).

Isolated single-cell convection, which can also be referred to as "pulse-style"

convection, is driven more thermodynamically than dynamically. The buoyancy needed

for pulse-style convection to occur is mostly due to the diurnal cycle, as opposed to

synoptic forcing features (such as fronts). Normally, this type of convection resides in

environments with low values of bulk (0-6 km) vertical shear (< 10 m s^{-1}). The

maximum updraft for tropical convection with weak forcing (a quasi-minimum value for

maximum updraft speeds overall) is 5 m s^{-1}. It can be as high as 40 m s^{-1} in the midlatitudes. Pulse-like storms propagate individually and in no organized fashion with respect to the formation of any new pulse-like storms. Finally, updrafts in pulse-like convection are driven by buoyancy alone.

Multicellular convection is more organized than pulse-like single cells. New storms form in preferred areas along the gust front, and storm propagation and system propagation may be two different directions. The environment for multicellular convection is a moderate shear zone (~10-20 m s^{-1}) and can have a wide range of convective available potential energy (CAPE) available for storm formation. The cold pool and environmental horizontal shear interact to intensify uplift and cell propagation along the gust front.

Supercellular convection is the most organized and strongest form of isolated convection. Supercells usually occur in environments with strong bulk shear (> 20 m s^{-1}). They contain inflow lows that help induce updrafts. The cells propagate off of the mean wind vector (right of the vector for cyclonically rotating updrafts, left of the vector for anticyclonically rotating updrafts), usually caused by the combination of nonlinear (storm-splitting) and linear (enhancement/destruction of the split storms) dynamic forcing. The main feature of a supercell is the presence of a mesocyclone, which is a rotating updraft which is found to have vertical vorticity $O(10^{-2}\,s^{-1})$ which is present through at least half of the storm depth. Lofting and tilting of horizontal vorticity cores (caused by vertical wind speed shear) leads to formation of mesocyclones in supercells.

MCS's are very large, contiguous areas of deep convection. The length of an MCS is large enough that Coriolis effects are significant $O(100\ km)$. Cell propagation

within an MCS is similar to that of a multicell, but on a larger scale. MCSs often form in areas of strong synoptic forcing (i.e., fronts, drylines) than do QISCs. MCSs can form on their own, or, also as likely, form by upscale growth from one of the QISCs once a strong cold pool has been established in an environment favorable for MCS development. MCS environments tend to have at least moderate to strong shear (> 10 m s^{-1}), though that shear must be present through a deep layer. One characteristic of an MCS is the presence of a rear inflow jet, which aids in the strengthening of the cold pool and the downdrafts in the storm. An MCS may contain supercells embedded in the circulations of the MCS.

The main consideration for this study is how the two regimes are dynamically different in terms of their abilities to transport mass. Isolated single cells and multicells tend to have weaker updrafts, meaning that mass would not be able to be lofted as high as, for example, a supercell. Also, entrainment of environmental air into the updraft of a single- or multi-cell would dampen not only the updraft (due to evaporation caused by the intake of dry air into the storm), but any chemicals within the environmental air may react with chemicals that are being lofted. This would cause transport to also be lessened. For this study, since the tracers are completely passive, the latter of the two is not an issue. MCSs and supercells should both have more undiluted transport of chemistry to the UTLS region than multicells and single cells. Due to the rotation of the updraft in a supercell, entrainment of air into the updraft is lessened, protecting the core from dampening. In an MCS (Doswell et al. 1996) the environmental relative humidity (RH) around an MCS is usually high enough that the entrainment rates are severely reduced, allowing the updrafts in an MCS to be mostly undiluted.

CHAPTER III

METHODOLOGY

WRF Setup and Sensitivity Tests

This study employs the Weather Research and Forecasting (WRF) chemistry model (WRF-CHEM). The model version is WRF-CHEM 3.2.1, which utilizes the Advanced Research WRF (ARW) core. This study utilizes the passive tracers available in the model for transport. The ARW core utilizes fully compressible, non-hydrostatic forms of the Euler equations and is conservative for scalars (Skamarock et al. 2008). The full Coriolis terms are included in this model to ensure that the long-lived features that are affected by the Earth's rotation are properly handled. It has the option for one-way or two-way interactive grid nesting, with the current study utilizing the latter of the two. North American Regional Reanalysis (NARR, Mesinger et al. 2006) data, which are provided every three hours, are used to provide the initial and lateral boundary conditions.
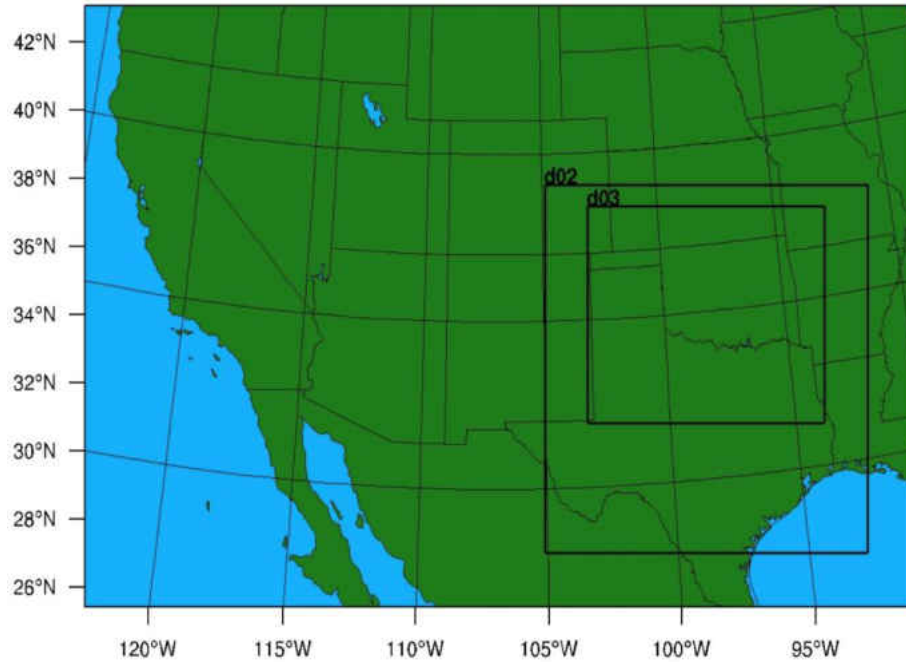
Fig. 3. Borders of the domains used in the study for the majority of the scientific exploration. The entire outline around the plot is the edge of domain 1, and labeled are the nests d02 and d03.

A parent grid having two nests with grid spacing of 18, 6, and 2 km is used for most of the simulations (Fig. 3). The 2-km grid spacing domain is the analysis domain that is used for analysis herein. The parent grid has 176x112 grid points in the x and y directions, respectively, and the nests have 205x205 and 442x352 grid points. The centermost point for the parent grid is over New Mexico, but the focus area of the current study is the state of Oklahoma (Fig. 3). This was chosen as the area of interest due to the vast amounts of surface observation and radar data available there for model verification. The simulations utilize 46 vertical levels (Fig. 4). These levels are mass vertical levels denoted by η (eta), a terrain-following sigma-hybrid coordinate ranging from 1.0 at the surface to 0 at the model top. To better resolve updraft entrainment and detrainment, the levels were explicitly defined to provide greater resolution in the boundary layer (~0-3

33

km), and in the area of expected detrainment from convective updrafts (~8-13 km). Although most WRF simulation studies have high vertical resolution in the boundary layer, the increased resolution aloft is relatively unique. From approximately 6 km to 8 km AGL, the vertical spacing decreases from ~750 m to 250 km. From approximately 8 km to 12 km, the levels are equally spaced at 250 m. Above approximately 12 km, the domain spacing stretches back out to ~750 m in the same manner in which it compressed.
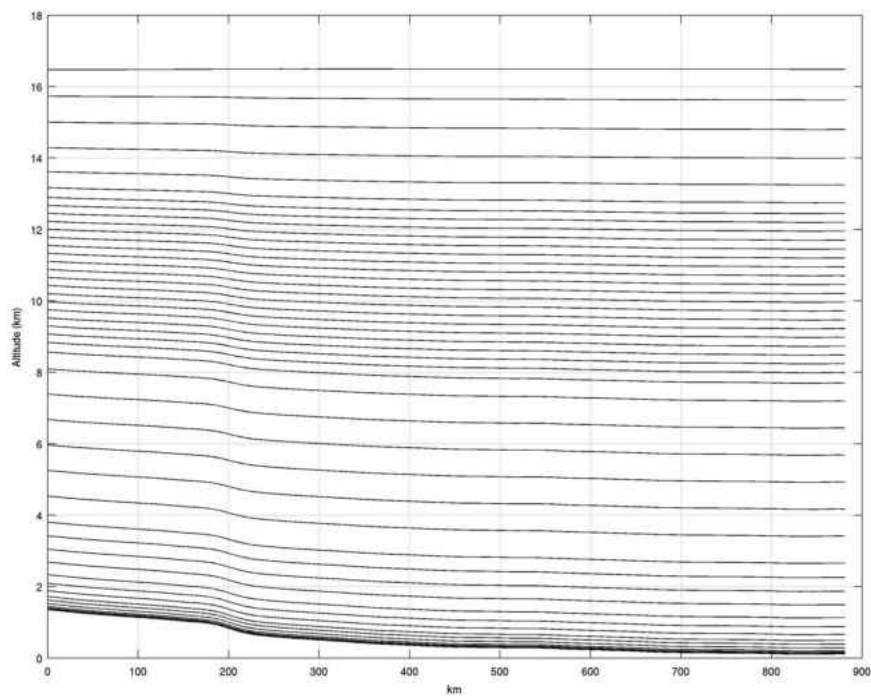
Fig. 4. Cross-section of the vertical levels utilized in the WRF simulations for the study. This figure shows the intentional stacking of levels in the boundary layer and around the tropopause region. Note that the vertical axis of this plot is in km MSL and not AGL.

The analysis time period for the current study was 15-31 May 2007 and 1-13 July 2007. This corresponds to 17 analysis days in May and 13 in July. The reason for analyzing storms during 2007 is that 2007 was a relatively actively convective year for the Southern Great Plains (SGP) region. Analyzing storms in May and July allows for

the study to capture storms that exist in two dynamically different environmental regimes. On the average, May exhibits mostly a shear-zone convection environment, in which many frontal systems and dry-line setups are common during the period. This lends to more organized convection being common during this part of the convective season. In July, the environment is more of a subtropical warm-sector, and the convection is more thermodynamically driven than in May. Though frontal systems and dry-lines are still possible during this part of the season, it is much less common than in May for the region. As such, more pulse-like convection and convection that is less-organized is more common.

Table 1. Model configuration and physics parameterizations.

Model	WRF-CHEM Version 3.2.1
Longwave Radiation	Rapid Radiative Transfer Model (RRTM)
Shortwave Radiation	Dudhia
Microphysics	Thompson Single-Moment
Cumulus	Grell Ensemble
Planetary Boundary Layer	MYJ
Surface Layer Physics	MYJ
Surface Physics	Unified Noah Land-Surface Model

As discussed in Chapter 2, WRF has numerous physical parameterization options. A summary of the WRF-CHEM physics configuration used herein is provided in Table 1.

There is no one perfect parameterization configuration as each individual scheme

produces errors and, when combined with other individual schemes in the different areas,

produces errors in the interactions between schemes as well. To mitigate this problem,

testing of different schemes and their interactions is necessary to determine the best

configuration. In this project, the best configuration was defined by the model's ability to

reproduce realistic conditions for various flow regimes. Evaluation criteria were based

mainly on the structure of the model derived radar reflectivity field.
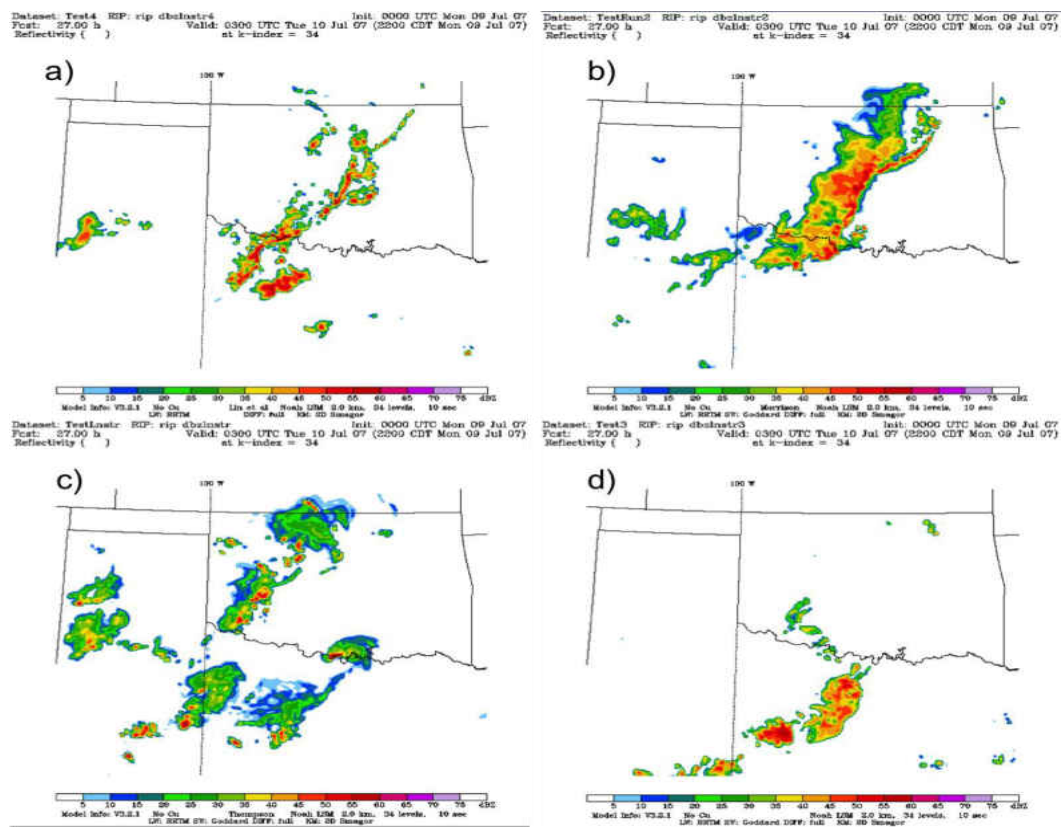
Fig. 5. Model-derived radar reflectivity for the study domain at 0300 UTC on 10 July
2007. A) is the Lin scheme, b) is the Morrison scheme, c) is the Thompson scheme, and
d) is the WRF double-moment scheme.

Basic evaluation of different parameterization configurations was conducted using

both a squall line convective case (which was considered to be "strongly forced" by a

cold front, as in Fig. 5) and a warm-sector convection case (which was considered to be "weakly forced", as in Fig. 8). To determine the best configuration, a single parameterization was changed (e.g. convective parameterization) while holding all other model configuration choices constant, and the ability of the model to reproduce observed radar reflectivity structures was assessed. From there, the best parameterization was chosen and held constant while the next parameterization was changed.

The schemes that were changed were the microphysics and PBL (and attendant surface layer and surface physics) schemes. The amount of spin-up time was also changed. The first run was started at 6 hours before the convective event took place. This time difference allows the model to "spin-up" all of the parameterization schemes and the model dynamics to start producing realistic conditions. After that run, three hours were added to the start of the run for more spin-up time, and then six. The best run of the three was chosen and the associated amount of spin-up time was used.
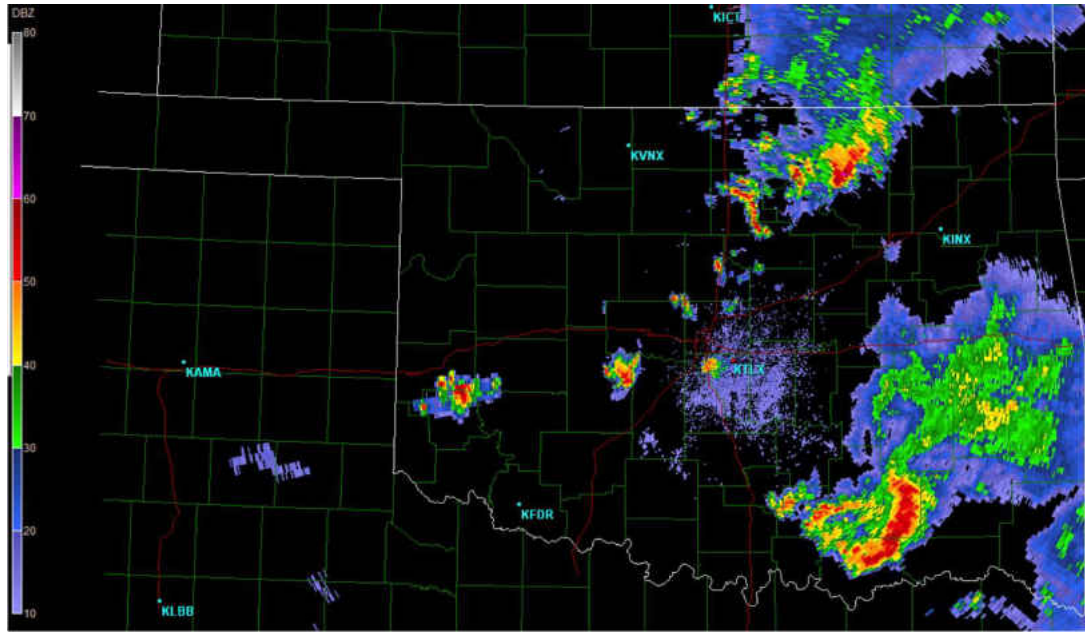
Fig. 6. NEXRAD radar base reflectivity data from the Norman, OK radar (KTLX), at 0302Z on 10 July 2007.

The first parameterization tested was microphysics. The four parameterizations used were the WRF 6-class double-moment scheme (Skamarock et al. 2008, and references herein), the Morrison double-moment scheme (Morrison et al. 2005), the Lin single-moment scheme (Lin et al. 1983), and the Thompson single-moment scheme (Thompson et al. 2004). Since atmospheric models tend to displace convection in both space and time when compared to observations, a qualitative assessment of the "best" parameterization was done by first analyzing the structure of the convection at a certain time with a certain storm type and comparing the schemes. Of course, as stated below, this is not the only method that this determination was done. In the case presented in Figs. 5-7, a mesoscale convective system (MCS) is present within the domain. Neither the double-moment WRF scheme nor the Lin scheme produced any stratiform-like areas of reflectivity (Fig. 5 a,d). The Morrison scheme produced a stratiform-like area on the

north end of the storm, as well as the two weaker systems following behind the storm

(Fig. 5 b). The simulation that utilized the Thompson scheme (Fig. 5 c) produced the

most realistic-looking results (when compared to the system in Fig. 6). The line was

somewhat broken, and where there was a strong line of convection there was a trailing

area of stratiform-like returns.
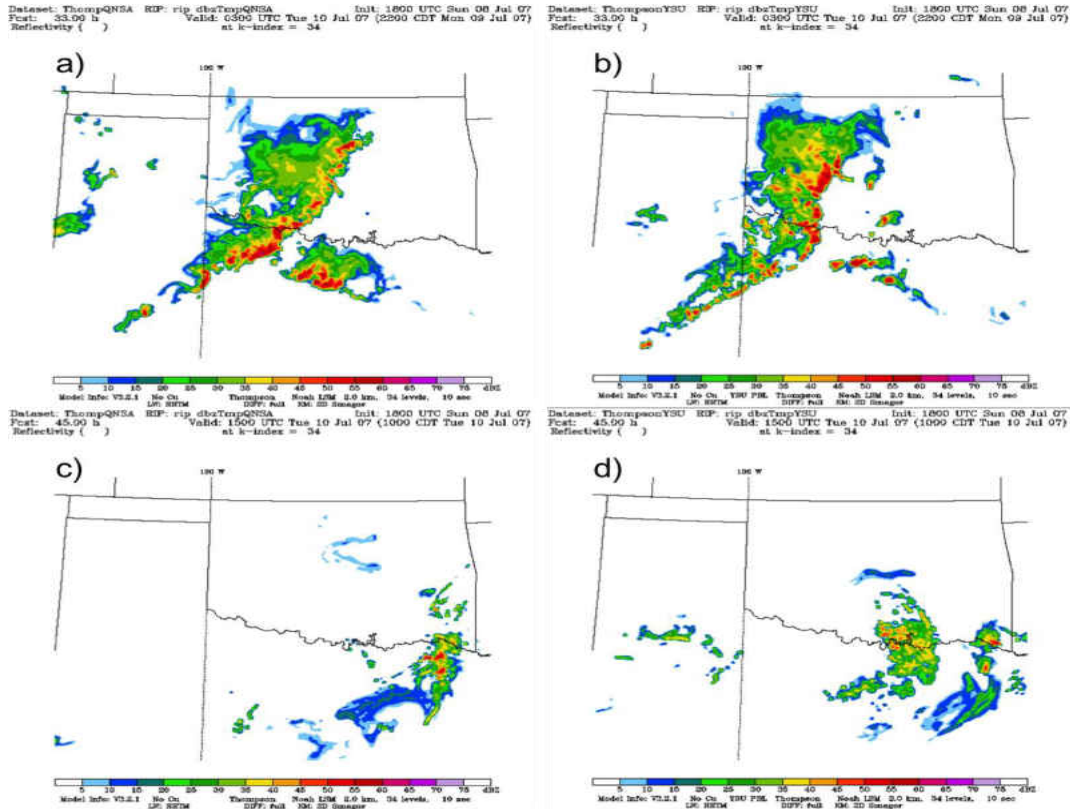
Fig. 7. Model-derived radar reflectivity for the study domain at 0300 UTC on 10 July
2007 (a and b), and 1500 UTC on 10 July 2007 (c and d). Shown are a) the QNSE PBL
scheme at 0300 UTC, b) the YSU scheme at 0300 UTC, c) the QNSE scheme at 1500
UTC, and d) the YSU scheme at 1500 UTC.

Next, the boundary layer scheme was varied between three different schemes, and

again validated using modeled radar reflectivity. The schemes that were tested are the

Quasi-Normal Scale Elimination PBL scheme (QNSE, Sukoriansky et al. 2006), the

Yonsei University scheme (YSU, Hong et al. 2006), and the Mellor-Yamada-Janjic PBL

scheme (MYJ. Janjić 2001). The structural differences of the convection due to changes in boundary layer parameterization (Fig. 7) were not nearly as significant as those that arose with changes of the microphysics schemes. The structural differences are most likely due to changes in the heating profiles and the boundary layer height, as the storms are rooted within the boundary layer and any changes to heating will affect their structure. Comparing surface temperatures was another method in which the sensitivity was analyzed. Surface temperatures seemed to coincide fairly well with the observations for the MYJ scheme, and the modeled radar reflectivity structure shows similar characteristics to that of the observed radar returns (Fig. 8).
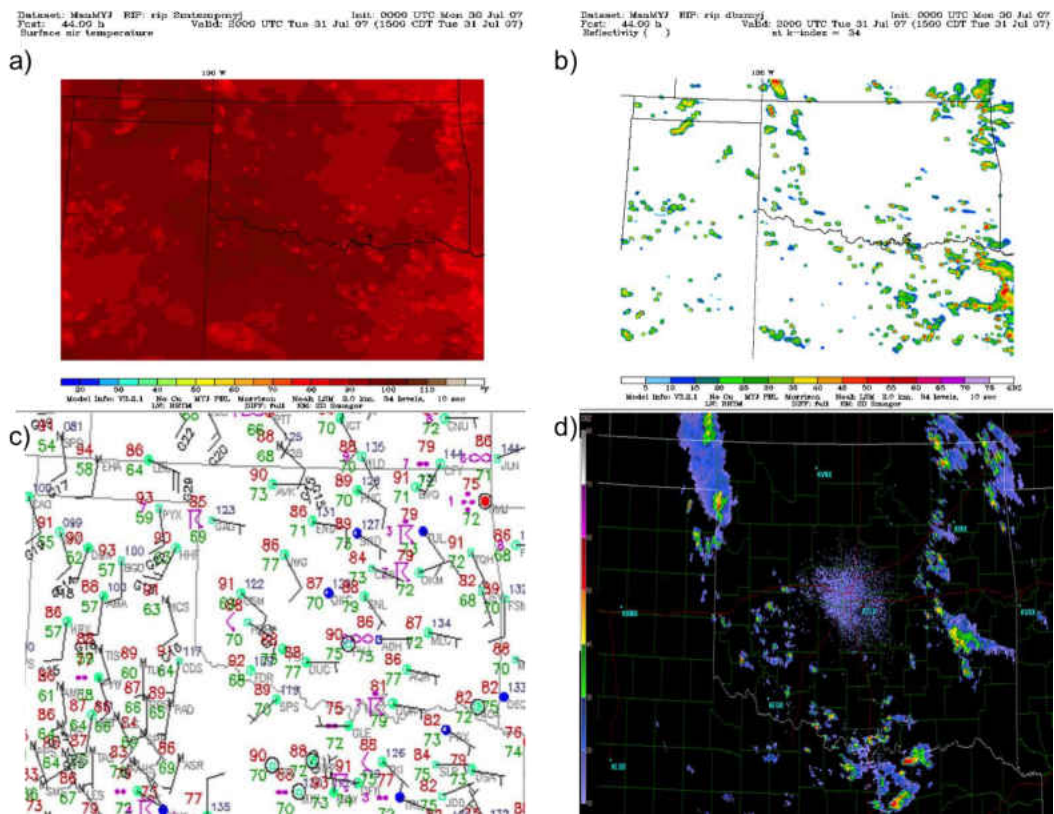
Fig. 8. Composite plot from around the 2000 UTC time on 31 July 2007. A) 2 m temperatures using the MYJ PBL scheme, b) is a plot of model-derived radar reflectivity at the same time, c) is a plot of observations taken from the UCAR RAP page at the same time, and d) is the NEXRAD base reflectivity from the Norman, OK radar (KTLX).

40

The configuration of WRF utilized in the current study uses the following parameterizations: Grell-Devenyi ensemble cumulus parameterization scheme (Grell and Devenyi 2001), Thompson single-moment microphysics scheme (Thompson et al. 2004), and the MYJ PBL scheme (Janjić 2001).   Also, a spin-up time of 6 hours was chosen for the study from testing and for consistency with previous research (e.g., Skamarock 2004; Weisman et al. 2008; Aligo et al. 2009), which found that some model errors are mitigated and convection can be reasonably reproduced 3-5 hours form model initialization. It is to be noted that this amount of spin-up time may not be sufficient for all simulated meteorological situations, but is reasonable for the current study.

Once the initial parameterization choices were made, a longer case was chosen (eight full days of runs compared to two full days) that introduced some variability in the convective regime and also enabled testing model time/restart frequency. The convective regimes included in the eight-day period of 8-15 July 2007 included no convection, squall line and warm sector convection. The model was reinitialized every 48 hours with a 6-hour overlap between runs so that no spin-up time would be used in the analysis. Subjective analysis (not shown) of model derived radar reflectivity during the period showed that the simulated variability in convective mode (MCS's, multicells, warm-sector single-cell convection, no convection during heating hours) matched the variability seen in the observations, so the chosen model physics options and re-initialization frequency should be sufficient to capture convective variability over longer periods of time.

Classification of Thunderstorms

The intent of the current study is to determine if a relationship between storm type and convective mass transport can be quantified, so an objective storm classification scheme is needed. Building off of the Schoen and Ashley (2011) classification scheme, convective objects were identified and sorted based on modeled radar reflectivity. As stated in the previous chapter, many existing classification schemes subjectively evaluate radar reflectivity, but a completely objective scheme was utilized for this study. In addition, although not used in the primary regime classification, updraft strength and depth was used for evaluating certain storm features in the final analysis.

The first step in classifying storms is calculating radar reflectivity factor on the output grid at every output time. This is done using the mixing ratios of rain, snow and graupel, following the formulation given in the Read/Interpolate/Plot (RIP; Stoelinga, 2013) software. The mixing ratios of rain, snow, and graupel each have a certain weight, since for the same concentration of particles, each type has a different reflectivity. Each type is multiplied by its weight to attain a partial reflectivity and then the three values are summed to produce the total reflectivity.

Table 2. Thresholds used for object determination in the MODE tool.

Parameter	Threshold
Threshold Applied to Raw Data	> 0 dBZ
Convolution Radius of Influence	9 Grid Squares
Threshold for Bad Data (Throw out objects with > n % bad data)	50
Threshold Applied to Convolved Data	≥ -15 dBZ
Areal Threshold (Ignore objects smaller than threshold)	0 Grid Squares

Calculated reflectivity values include the effect of bright banding by identifying snow particles in the melting layer (based on temperature) and adjusting the reflectivity for that layer. The three-dimensional reflectivity field is then interpolated to 1 km AGL.
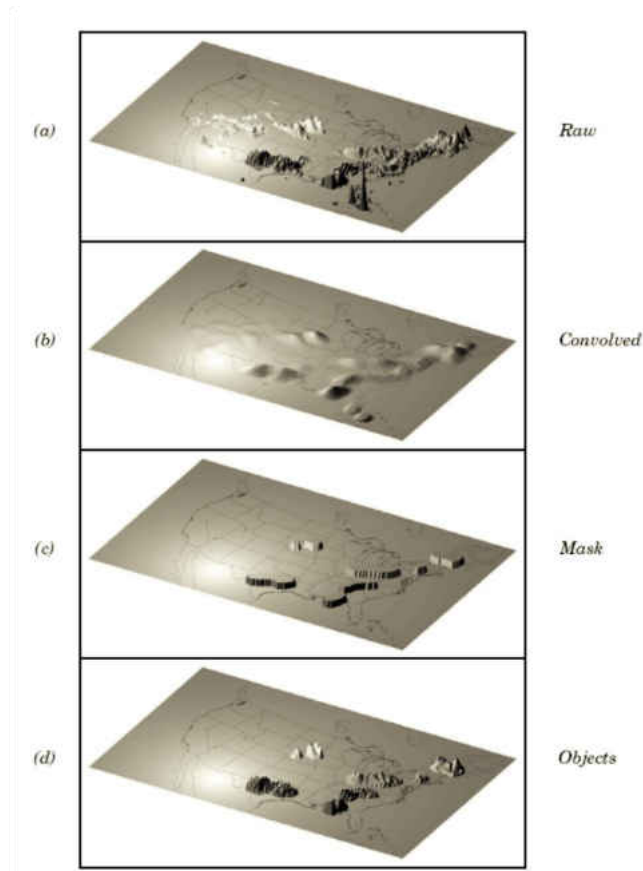
Fig. 9. Figure from Brown et al. 2007. Process by which object determination is performed in the MODE tool. A) the raw precipitation field given. B) field when the circular convolution is applied to the raw field. C) objects created by applying the masking field to the convolved field. Finally, d) raw field being placed back onto the map in area given by the mask field, thus creating the object.

Model reflectivity values are then written to a format compatible with the Meteorological Evaluation Tools' (MET) Method for Object-Based Diagnostic Evaluation Tool (MODE) (e.g. Davis 2006 a,b; Brown et al. 2007). Version 3.0 of MET was used in the current study. MODE uses convolution thresholding to resolve objects given a raw data field. The data are passed through a filter function given by

$$C(x,y) = \sum \phi(u,v) f(x-u)(y-v), \tag{3.1}$$

where C is the convolved field (Fig. 9b), ϕ is the filter function, (x,y) and (u,v) are coordinates on the grid, and f is the raw data field (Fig. 9a). The filter function is defined as

$$\phi(x,y) = H \quad \text{if} \quad x^2 + y^2 \leq R^2, \text{ and } \phi(x,y) = 0 \quad \text{otherwise.}$$

Here, H is a height and R is a radius of influence. The radius of influence of the filter function is set by the user and is determined using

$$\pi R^2 H = 1. \tag{3.2}$$

Once the convolution is performed, the newly convolved field is then masked using a threshold for how much of the object to keep (Fig. 9c). This is given by

$$M(x,y) = 1 \quad \text{if} \quad C(x,y) \geq T, \text{ and } M(x,y) = 0 \quad \text{otherwise.} \tag{3.3}$$

In (3.3), M is representative of the mask field, which is determined by knowing whether or not the convolved field, defined in (3.1), is above the user-defined threshold T. Finally, the raw data field is fed back in by multiplying the field, f, by M (Fig. 9d). This creates the objects that are then analyzed. The thresholds defined for the current study are given in Table 2. An example case from 15 May 2007 at 1200 Z is shown (Fig. 10) to illustrate the process for real data.
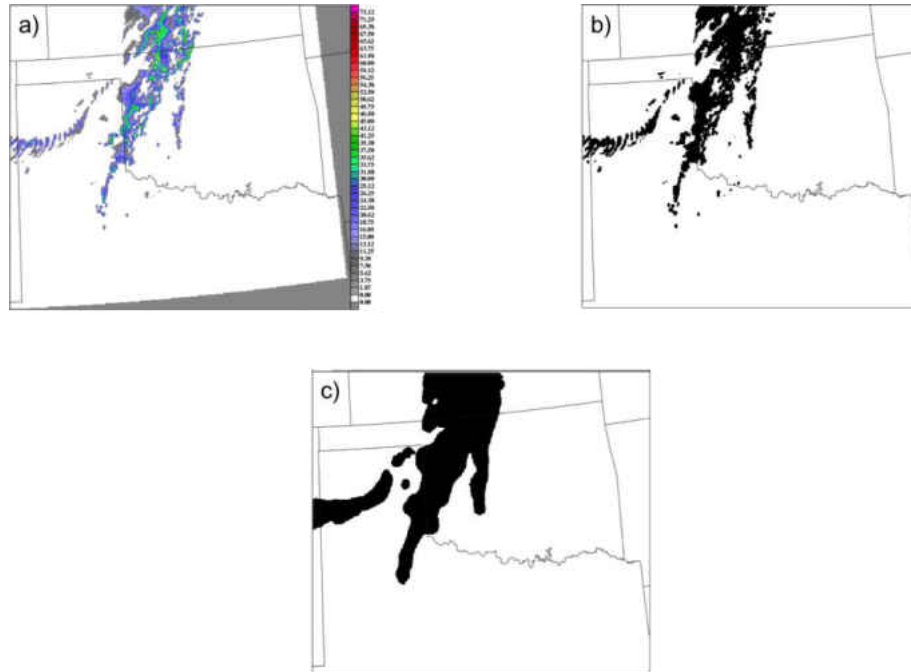
Fig. 10. Illustration of the process of object determination in MODE using a case from the current study. A) raw model-derived radar reflectivity of a storm system moving through Oklahoma. B) the field as declared objects in MODE, before convolution. C) what the object field looks like once the circular convolution and masking are applied to the field, as shown in Fig. 9.

The MODE tool outputs attributes associated with each object; the attributes used in the current study are the length, width and area of the object. The length and width are determined by calculating the aspect ratio, where a rectangle is defined by alignment with the axis angle and made just large enough to enclose the object. From there the minimum and maximum axes are found, and attributed to the width and length, respectively. The area is determined simply as a count of the grid squares that are contained within the object. Then, the true area can be determined by multiplying the count by Δx and Δy. From the example presented above in Fig. 10, for example, the length of the object is 554 km, the width is 273 km, and the object area is 67476 km^2. Note that the area of the object outlined in Fig. 10c is different than the actual reflective area of the cells contained

within the object, as the MODE-resolved object includes all of the "white space" of no

reflectivity around the areas of > 0 reflectivity. The reflective area (used in the

classification scheme for the current study) is 39816 km^2.

Table 3. Breakdown of each regime used in the classification scheme and the attendant
characteristics.

	Weak Convection (WC)	Quasi-Isolated Strong Convection (QIS)	Mesoscale Convective System (MCS)	Linear Mesoscale Convective System (LMCS)
Radar Reflectivity Characteristics	< 40 dBZ everywhere in object	≥ 40 dBZ at least 1 point in object	≥ 40 dBZ at least 1 point in object	≥ 40 dBZ at least 1 point in object
Areal Characteristics	Can be any size	< 7000 km^2	≥ 7000 km^2	≥ 7000 km^2
Axis Ratio Characteristics	Can be both linear and non-linear	Can be both linear and non-linear	< 4 length to width	≥ 4 length to width

The output from the MODE tool is then fed into the storm classification scheme

developed for this study. As mentioned above, the basic elements of the scheme are

based upon the classification scheme of Schoen and Ashley (2011; discussed in Chap. 2).

The scheme utilizes the model-derived radar reflectivity of objects as determined with the

MODE tool. Four classification regimes are used: weak convection (WC), quasi-isolated

strong convection (QISC), non-linear MCS (MCS) and linear mesoscale convective

system (LMCS), as shown in Table 3.

The first discriminator between classes is the strength of the radar reflectivity. If the radar reflectivity is below 40 dBZ for a given object, it is classified as WC (Fig. 11, Table 3). Any object that has reflectivity equal to or greater than 40 dBZ is then deemed to be in one of the three "strongly convective" classes (QISC, MCS, LMCS) and is passed on to the next evaluation criterion. For initial testing, only one point in the entire object needed to have a reflectivity value greater than 40 dBZ to satisfy the condition for being in one of the strong regimes.
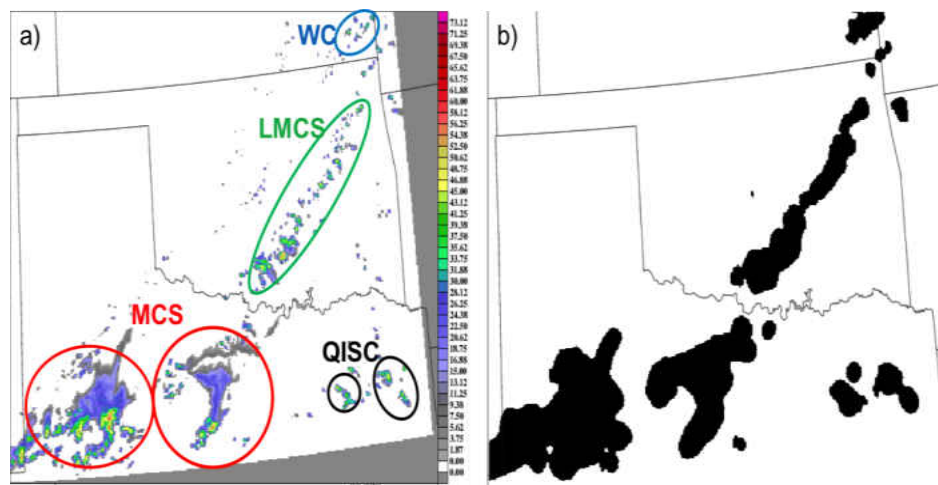
Fig. 11. Example case illustrating MODE object determination and classification scheme applied. A) the raw model-derived reflectivity field. Outlined are objects classified to each of the regimes. The blue circle outlines a weakly convective (WC) object, the black circles outline a quasi-isolated strong convection (QISC) object, and the red circle outlines a Mesoscale Convective System (MCS). A linear MCS is outlined in green as well. B) the attendant objects as identified by the MODE tool.

The next evaluator is the area of the object. This evaluation discriminates between MCS/LMCS and QISC. Being strong with respect to radar reflectivity and having an object area less than 7000 km2 defines a QISC. Any object with an area greater than or equal to 7000 km^2 then passes on to the final evaluation criterion and is classified as one of the two MCSs (Fig. 11, Table 3). This spatial area criterion is larger than the size requirement for MCS's as defined in Houze (1993), which is that the MCS

48

has length on a side of at least 100 km, and assumedly the other axis length is about 10 km. The criterion used in Houze (1993) does not work for the current study, as the entire reflective area is used in the classification of the MCS, whereas in Houze (1993), the areal threshold is confined to the actively convective area, separating it from the stratiform precipitation areas.

To determine whether an MCS is linear or non-linear, the axis ratio is used as the final classification criterion. If an object has an axis ratio of greater than or equal to 4, which is similar to yet smaller than Bluestein et al. (1987), then the storm is classified as a LMCS. If it is less than 4, the storm is classified as a non-linear MCS.

To be able to meaningfully analyze the tracer transport characteristics of classified storms, a dominant class is defined for each hour (the model output time increment). This is meaningful because a dominant class allows for analysis of the environment and other parameters that can be directly attributed to that specific class. The dominant regime is defined using a class' areal coverage percentage and whether this value exceeds a threshold value. Initial sensitivity testing showed that it was most meaningful to have a percentage threshold of 60% for a class to qualify as dominant. If no individual class satisfies this criterion, then the dominant class is said to be "mixed" (Fig. 11). When convection is "mixed", no truly meaningful analysis can be performed at that time, and thus these times are not included in the analysis.

Sensitivity Tests on Classification Parameters

Many parameters in the classification scheme are tunable and can greatly impact the results. For this study, two such parameters were analyzed. Those parameters were

49

the areal threshold and the amount of points necessary for an object to qualify as one of the three strongly convective regimes. The areal threshold is used to discriminate between the MCS regimes (both MCS and LMCS) and the QISC regime, and is based on the size of the entire object, not just the actively convective regions. The threshold for the number of points of strong convection in an object controls the determination of whether an object is WC or if it belongs in any of the three other regimes.

a. Areal Threshold

Initial testing utilized a threshold of 2000 km^2 for the area of the object, which corresponds to a square approximately 45 km on a side. Results from that initial testing showed that, subjectively, objects that were being classified as MCSs would not have been classified as such with a subjective classification method. Therefore, five additional size thresholds were tested: 5000, 7000, 10000, 13000 and 15000 km^2 (Fig. 12).
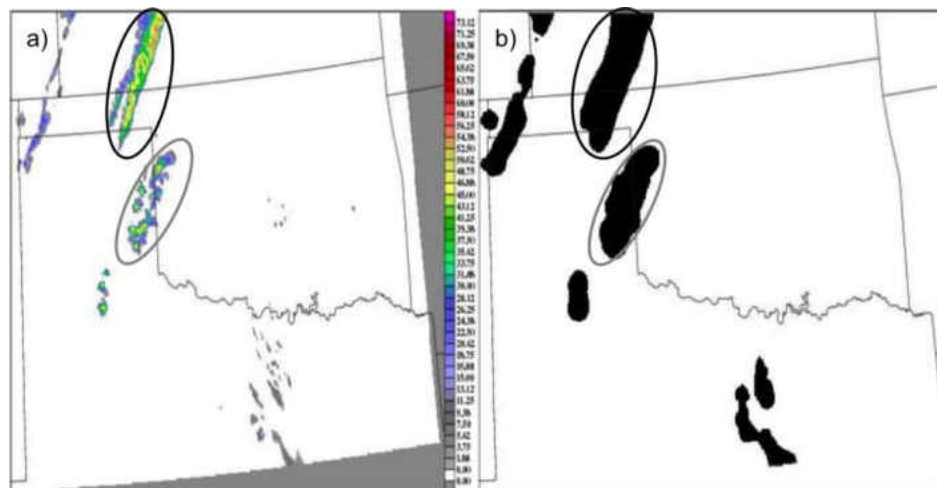
Fig. 12. Example case from 24 May 2007 at 0500Z. A) Model-derived radar reflectivity field, and B) MODE-derived objects, both as in Fig. 11. Two different storms are encircled in black and grey in both (a) and (b).

Each of the chosen thresholds was implemented on the entire analysis time period. Subjective analysis of many individual cases where storms were classified as an

MCS with the lower threshold and a QISC with a threshold of interest was used to determine whether a tested threshold was "better". If a storm in question was classified as an MCS at the analyzed threshold and subjectively determined to not resemble an MCS, it was noted. After analysis of many cases, if the majority of the storms did not resemble MCSs, then the threshold was increased and the same method was applied to the next threshold.

After testing each of the thresholds, the "best" thresholds were determined to be the 7000 and 10000 km^2 levels (Fig. 12, object circled in black). Since the top two were chosen, more testing had to be performed. This is because without such testing, it is unknown if the two chosen thresholds are indeed the ideal ones for the study, or if any higher threshold would be better. As such, 13000 and 15000 km^2 were also tested. After testing these thresholds, subjective analysis determined that 7000 and 10000 km^2 were the best thresholds (Tables 4-5). The reason for this is that, conversely to having too small of a threshold in which subjective QISC were classified as MCS (Fig. 12, object circled in grey), for the extra thresholds, storms that would subjectively be classified as MCS were classified as QISC (Fig. 12, object circled in black). Tables 4-5 quantify the sensitivity of dominant regime hours to this threshold. There are fairly big jumps in the QISC (13-28-45) and MCS (204-185-154) in July between 5000 km^2 and 10000 km^2. In May the differences between thresholds are much smaller. This study utilizes the 7000 km^2 threshold. It is of note that some objects that are on the domain edges may in fact be quite bigger than calculated, and as such at some times one may not be capturing the whole storm and may be misrepresenting its true class.

Table 4. Number of hours where each regime was dominant for each of the tested areal thresholds, for May.

Object Reflective Area (km²)	No Convection	WC	QISC	MCS	LMCS	Mixed
2000	5	106	10	220	0	43
5000	5	106	24	196	0	53
7000	5	106	38	183	0	52
10000	5	106	57	164	0	52
13000	5	106	79	140	0	54
15000	5	106	94	124	0	55

Table 5. Number of hours where each regime was dominant for each of the tested areal thresholds, for July.

Object Reflective Area (km²)	No Convection	WC	QISC	MCS	LMCS	Mixed
2000	11	25	19	208	0	43
5000	11	25	63	156	0	51
7000	11	25	92	138	0	40
10000	11	25	124	113	0	33
13000	11	25	145	98	0	27
15000	11	25	156	93	0	21

b. Number of Points Required to Qualify as Strong Convection

Initially, an object only needed to have a single point in the entire object that had a reflectivity value above 40 dBZ to place that whole object into one of the strong convective classes. However, a very large object (e.g. > 10000 km² in area) that has as little as 1 to 3 grid points where the reflectivity is greater than 40 dBZ is unlikely to be

strongly convective. Even small objects (e.g. < 5000 km^2 in area) that have 1 to 3 points where reflectivity is greater than 40 dBZ are unlikely to be strong convective storms those points may be caused by processes other than deep convection.

To investigate this issue, when performing classification, storms were flagged if they contained three or less points in which the reflectivity was calculated to be greater than 40 dBZ. Then, flagged storms were analyzed to determine if a certain object size was more likely to be flagged or if it spanned a large spectrum of sizes. For the most part, smaller storms (less than 5000 km^2 in area) tended to be the ones flagged (477 of 496 storms), and a very small number of the cases flagged were large storms (greater than 25000 km^2), with only 4 storms of 496 being flagged. The other 15 storms had areas between 5000 km^2 and 25000 km^2. It was determined that the original method of just allowing a single point to count the object as strongly convective was a reasonable choice for the current study and is consistent with the methodology of Schoen and Ashley (2011). It is acknowledged that this is a parameter that can be studied and examined in further detail in the future to determine how best to apply to classification schemes.

Transport Analysis Methods

To explore the relationship between storm regime and transport characteristics, determination of the depth of transport and the magnitude of transport is necessary. The primary analysis method was to objectively estimate the magnitude of deep convective

transport in the domain. Specifically, vertical profiles of horizontally integrated tracer mass were created to ascertain desired quantities.

To ascertain the integration area, a deep convection condition must be determined. Deep convection has been defined in previous studies using varied vertical velocity thresholds (e.g. Xu and Randall 2001; Zhang and Wu 2003; Wu et al. 2009; DelGenio et al. 2012). For this study, conditions were subjectively established. The first condition is that the vertical velocity must be greater than 2 m s^{-1} at 4 km. This is used because that level should be within the updraft but also in the vicinity of the base of the updraft, as it was found that, especially in July, the PBL can be as deep as 4 km. The second condition is that vertical velocity be greater than 5 m s^{-1} at 8 km. At this level, the storm's updraft should be near its maximum. A column is deeply convective if both conditions are met for that given column. A test that added the condition that vertical velocity be greater than 1 m s^{-1} at the top of the model-derived PBL for a column to be deeply convective was conducted. Adding this condition drastically reduced the number of points considered to be deeply convective. In May, there were only 273 columns that met all three conditions, as opposed to 5338 columns that met the first two conditions. In July, only 228 columns met all conditions whereas 8185 columns met the first two conditions. With so few points meeting all three conditions for both months (5 % in May, 3 % in July), only the first two conditions were used in the current study to identify deep convection.
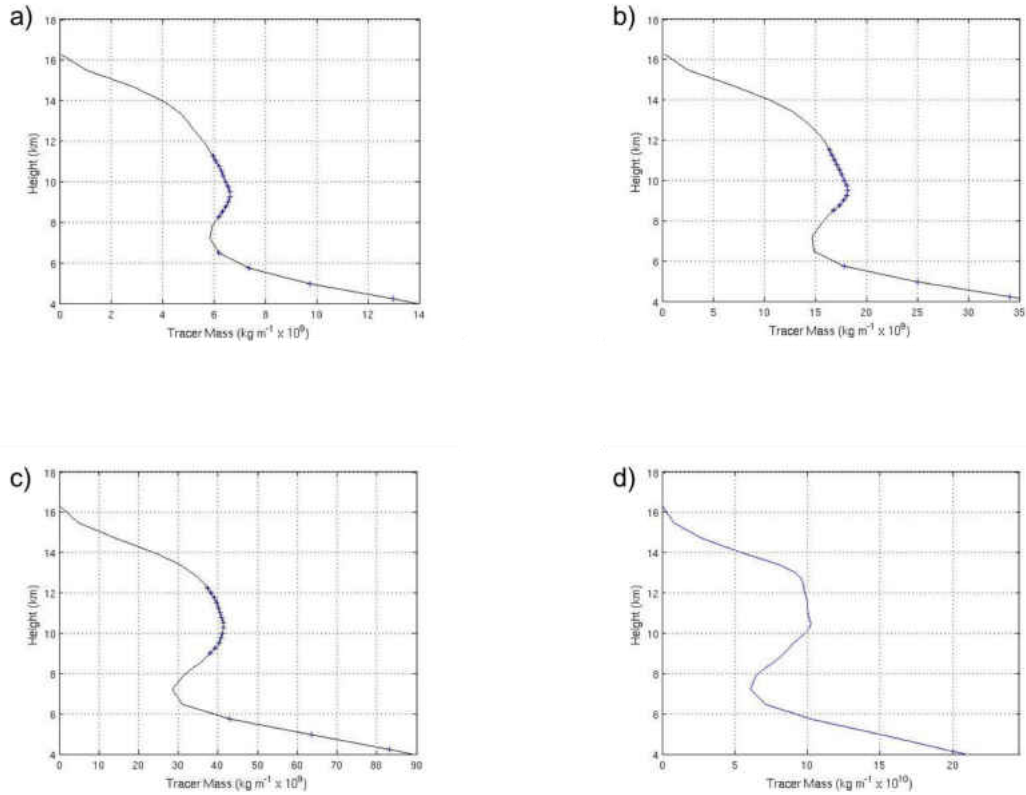
Fig. 13. Vertical profiles in altitude of calculated tracer mass. A) tracer mass using assumed 50 km square anvil area. B) tracer mass using assumed 100 km square anvil area. C) tracer mass using assumed 200 km square anvil area. Finally, d) tracer mass using entire domain for calculation. Calculated detrainment envelope shown by clustering of blue "+" in profiles. The profiles were calculated for the domain at 0600Z 13 July 2007.

Once deep convection is identified, an associated "anvil region" is delineated. The anvil region is estimated to be a square box centered on the convective core (Fig. 13). The convective core itself is excluded from analysis. The reason for this is that in the overshooting tops, the buoyancy is negative and therefore the transport is reversible. For this study, only the possibility of irreversible transport is considered, such as within the anvil region. For columns of deep convection for which the anvil regions would overlap, such a region is only counted once towards analysis. Figure 13 shows the changes in estimated tracer mass as a function of assumed anvil size tested for this study

(50 km square box, 100 km square box, 200 km square box, and entire domain, respectively). The 200 km square box was chosen as most representative of resolved convective outflow to ensure that the majority of the anvil area was covered, but at the same time help mitigate the possible problem of tracer contamination (Fig. 14). The tracer was initialized in the PBL for all three domains, and, with convection occurring on all three domains, any of the tracer lofted by convection on the outer domains can be advected into the analysis domain as smooth-looking tracer (see outlined area in black, Fig. 14) and cause calculations to be less robust.

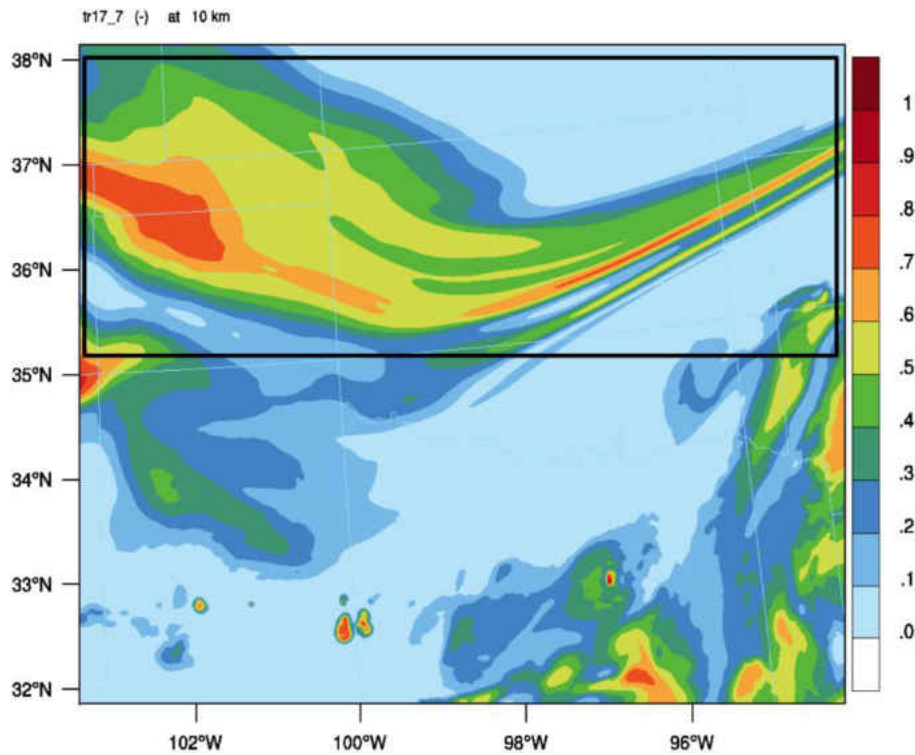Fig. 14. Tracer concentration hoizontal cross-section interpolated to 10 km AGL. Valid time for plot is 1200 UTC 16 May 2007.

Tracer mass was then calculated by taking the model output tracer concentration, which is a mixing ratio, and attaining mass per volume by multiplying the density of dry air. From there, multiplying by the horizontal grid area gives the desired mass per

altitude for each column. Each level is then integrated over the total horizontal anvil area (Fig. 13).

One of the quantities that can be estimated using these vertical mass profiles is the level of maximum detrainment (LMD; Mullendore et al. 2009, 2013). A critical point point in the free atmosphere at which the mass of the boundary layer tracer starts increasing after decreasing (approximately 7 km for domain analyzed in Fig. 13) is commonly present. This increase signifies deep transport. Above this critical point, the level at which the mass is a maximum is the mass-estimated LMD. An envelope is also determined around the LMD. This envelope consists of points where the mass is within 10% of the mass at the LMD, and was used mainly for subjective comparison of the vertical profiles and tracer cross-sections. In Fig. 13a-c the blue "+" identify the determined detrainment envelope. The estimated magnitude of transport, the other mass-based evaluation criterion, is calculated by simply integrating the mass from the inflection point to the top of the model.

Additionally, the altitude of the LMD is compared to that of the tropopause, as one would expect deeper storms when the troposphere is deeper, so calculating the relative depth helps normalize results for storms occurring in different seasons or different synoptic environments. This comparison provides a clearer picture as to which regimes have the potential to transport mass into the stratosphere. The tropopause is a layer that can be difficult to identify, as it is a fluid surface that can be greatly affected by perturbations such as thunderstorms. The World Meteorological Organization defines the tropopause as the point where the lapse rate falls below 2 K km^{-1} (which means the rate of change of temperature with height is becoming less negative) and where the average

57

lapse rate between that first level and 2 km above it is also below this threshold (World

Meteorological Organization, 1957). Others have defined the tropopause using potential

vorticity units (2 PVU, Holton et al. 1995), or using the gradient of θ ($d\theta/dz = 0.00935$ K

m^{-1}, Mullendore et al. 2005). For this study, the tropopause was attained from the NARR

dataset and is calculated to an interpolated geopotential height. The tropopause height

directly calculated from the model was not used because of the variability in the

tropopause height within the domain that is attributed to distortion by the complex

gravity wave motions and overshooting tops in deep convection. The data were available

every three hours. The method of tropopause identification used in the NARR data

comes from the first part of the WMO method.
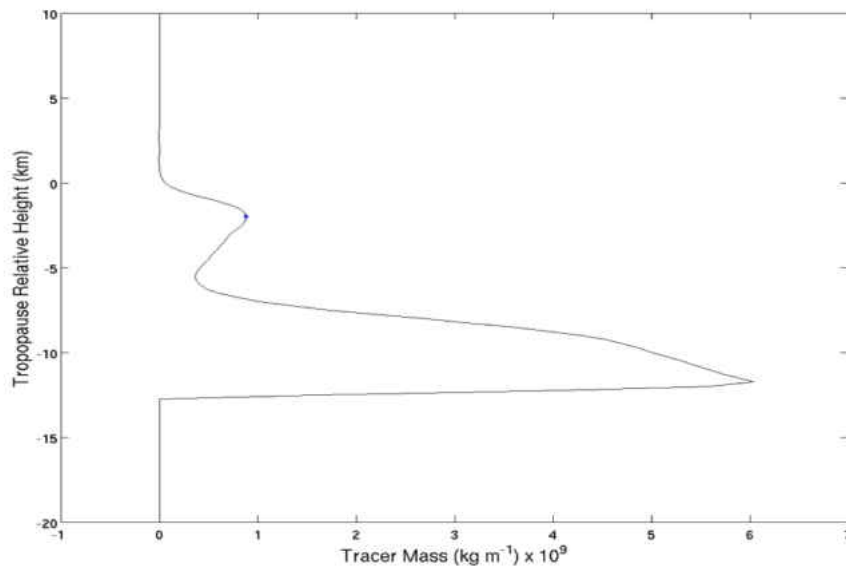
Fig. 15. Vertical profile of tracer mass with increasing altitude relative to the tropopause. The calculated LMD altitude relative to the tropopause is plotted as a blue asterisk. Example from 1100Z 15 May 2007.

For this study, a nearest neighbor method was used to assign tropopause heights

from the NARR data to analysis grid points. The data is ingested into the model in three-

hour windows. For example, if the model hour is 1200Z, the 1200Z NARR tropopause

data are assigned to the grid and used for 1200Z-1400Z. Then at 1500Z in the model the

1500Z NARR data are assigned, etc. Once the grid NARR heights are assigned, that

altitudes are subtracted from all altitudes in the column. The vertical mass profiles are

then plotted as described above (Fig. 13), except now the altitudes are shifted to being

relative to the tropopause. The LMD altitude relative to the tropopause is determined in

the same way that is described above (Figs. 13, 15). Figure 15 shows an example case

from 15 May 2007 at 1100Z, where the tropopause-relative LMD altitude as determined

through this methodology, was -2 km.

CHAPTER IV

RESULTS AND DISCUSSION

Storm Classification

WRF-CHEM was run for the dates of 15-31 May and 1-14 July, 2007. The

resulting 690 hours of output were analyzed with the objective storm classification

methodology detailed in Chapter 3. Tables 6 and 7 summarize the overall findings of the

classification analyses for the May and July simulations, respectively. The averages were

calculated for each regime individually; for example, Table 6 shows that the average

percentage of the model domain covered by convective objects (of all types) during the

183 hours classified as dominant MCS is 8.1%.

Table 6. Table showing the number of hours throughout the month of May in which the regime was dominant, the average percent of the model domain covered by objects for all classification days, that same average coverage in km^2 and the variance of that coverage, and the average percent of the model domain coverage by deep convection (using the vertical velocity thresholds as presented in Chap. 3).

May Classification Statistics

Dominant Regime	# Hours Dominant	Avg % Domain Covered	Avg Domain Area Coverage (km²)	Standard Deviation of Area Coverage (km²)	Avg Area of Domain Covered By Deep Convection (km²)
No Convection	5	0	0	0	0
Weak Convection (WC)	106	3.1	19313	31505	10.9
Quasi-Isolated Strong Convection (QISC)	38	1.5	9547	7184	50.8
Mesoscale Convective System (MCS)	183	8.1	50270	36811	151.6
Linear Mesoscale Convective System (LMCS)	0	0	0	0	0
Mixed Convection	52	5.8	36105	29985	97.9

Table 7. Table showing the number of hours throughout the month of July in which the regime was dominant, the average percent of the model domain covered by objects for all classification days, that same average coverage in km^2 and the variance of that coverage, and the average percent of the model domain coverage by deep convection (using the vertical velocity thresholds as presented in Chap. 3).

July Classification Statistics

Dominant Regime	# Hours Dominant	Avg % Domain Covered	Avg Domain Area Coverage (km^2)	Standard Deviation of Area Coverage (km^2)	Avg Area of Domain Covered By Deep Convection (km^2)
No Convection	11	0	0	0	0
Weak Convection (WC)	25	1.6	9736	11514	0.48
Quasi-Isolated Strong Convection (QISC)	92	1.9	12022	8573	42.2
Mesoscale Convective System (MCS)	138	6.4	39801	23433	112.8
Linear Mesoscale Convective System (LMCS)	0	0	0	0	0
Mixed Convection	40	4.3	26561	17961	47.1

For May, differences between the MCS and QISC classes are quite clear (Table 6). While the standard deviation of areal coverage is high for the MCS category, its average coverage is approximately 5 times greater (50270 km^2) than for the QISC class (9547 km^2). More important for the convective mass transport is the area covered by deep convective updrafts. The areal coverage of deep convection for the MCS category (151.6 km^2) is approximately 3 times larger than that of the QISC category (50.8 km^2).

The MCS class (183 hours) was also a much more frequent dominant class in May as opposed to the QISC class (38 hours).

For July, the differences are somewhat less than that for May (Table 7). The MCS class (39801 km^2) still has a greater average areal coverage of the storms than the QISC class (12022 km^2), an areal coverage that is a factor of 3.3 greater. The percentage of domain covered by convection for MCSs (6.4%) and QISCs (1.9%) are only loosely consistent with the 5% value that Steiner and Yuter (1995) found for average percentage of coverage by storms exhibiting strong reflectivities (greater than 40 dBZ) (Fig. 16). The average areal coverage of deep convection for the QISC class (42.5 km^2) is only about 37% of the average areal covereage for the MCS class (112.8 km^2).
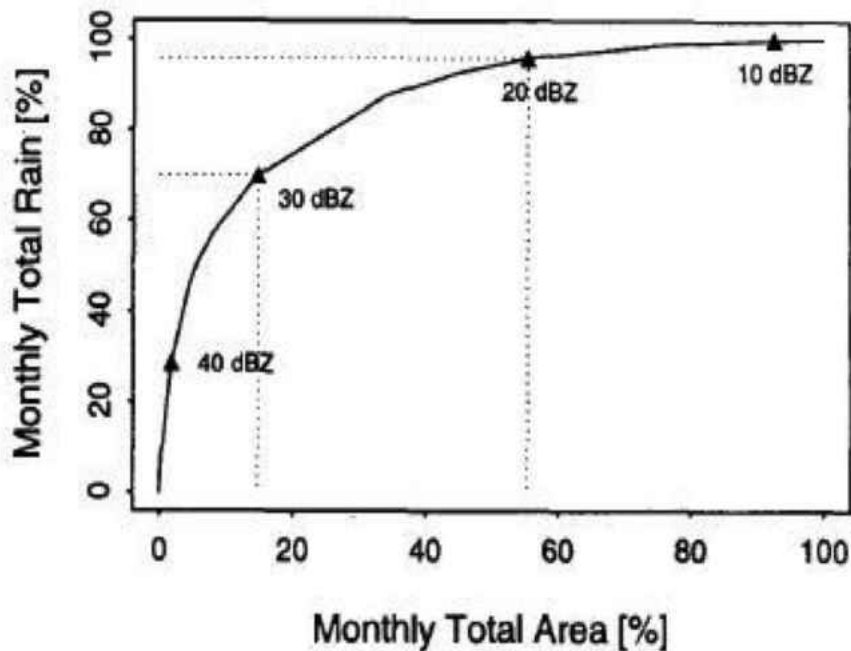

Fig. 16. From Steiner and Yuter (1995, their figure 17). This is an illustration of the contribution of radar reflectivity levels (labeled in increments of 10 dBZ and located by the triangles on the graph) to the monthly area covered (in percent) and the monthly total rainfall (in percent) for their data collected from Darwin, Australia in February, 1998.

Convective Transport Analysis

Following the methodology outlined in Chapter 3, the level of maximum

detrainment (LMD) and magnitude of mass transport were calculated for each hour (see

Fig. 13 in Chap. 3). LMD and mass transport magnitude time series were then

composited based upon dominant storm regime. Figure 17 shows the distribution of

LMD altitudes for the QISC and MCS regimes in May. Figure 18 shows the distribution

of the mass transport magnitudes for May, using the same plotting conventions as Figure
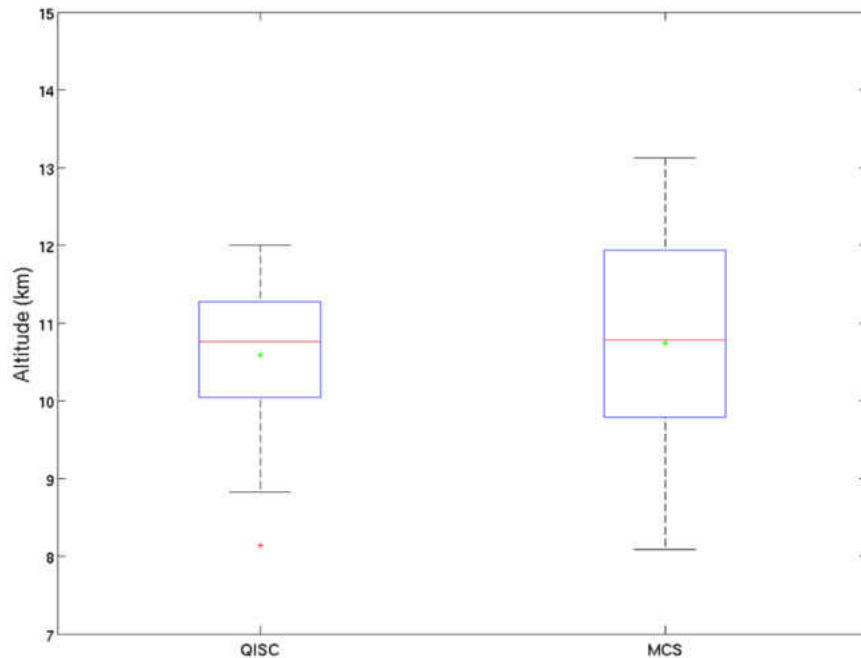
17.

Fig. 17. Distribution in the altitude to which mass was transported to the UTLS region by analysis of the LMD for May. The lower and upper bounds of the blue boxes represent altitudes at the 25% and 75% levels. The median value is the red line through the box and the green asterisk is representative of the mean value of the data. Outliers are denoted with a red plus sign.
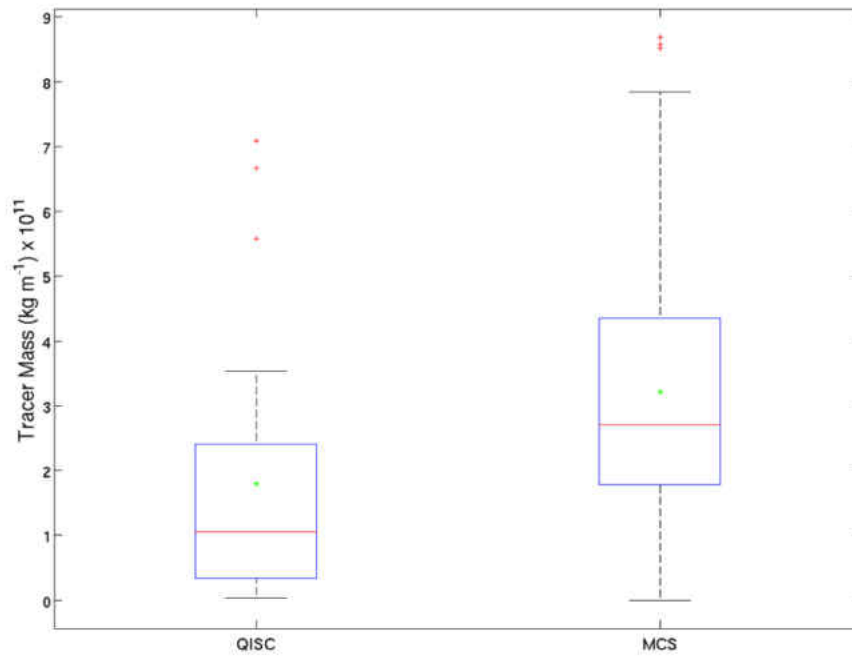
Fig. 18. As in Fig. 17, for the estimated magnitude of deep convective transport in May.

In May, there is no significant difference in LMD altitude for the QISC and MCS regimes (Fig. 17), as the mean values (10.59 km and 10.74 km, respectively) and median values (10.76 km and 10.78 km, respectively) are quite similar. Case examples are shown in Figures 19-22. Figures 29 and 21 show the model derived reflectivity for representative May QISC and MCS cases, respectively, with a line drawn through the planes where vertical cross sections of tracer concentration were plotted (Figs. 20, 22, left panel). Figures 20 and 22 (right panel) also show vertical profiles of tracer mass, plotted similarly to Figure 13, except that instead of an entire detrainment envelope being plotted on the profile, only the LMD is plotted as a blue asterisk. Figures 20 and 22 show that the anvils are constrained to the same general layer for both regimes (9.5 km to 12 km for

65

both cases), and, as shown in the right panels of Figures 20 and 22, the LMDs are located

at almost the same height for both regimes (10.77 km for MCS, 10.97 km for QISC).

This is consistent with the lack of difference in the distribution of LMD altitudes.
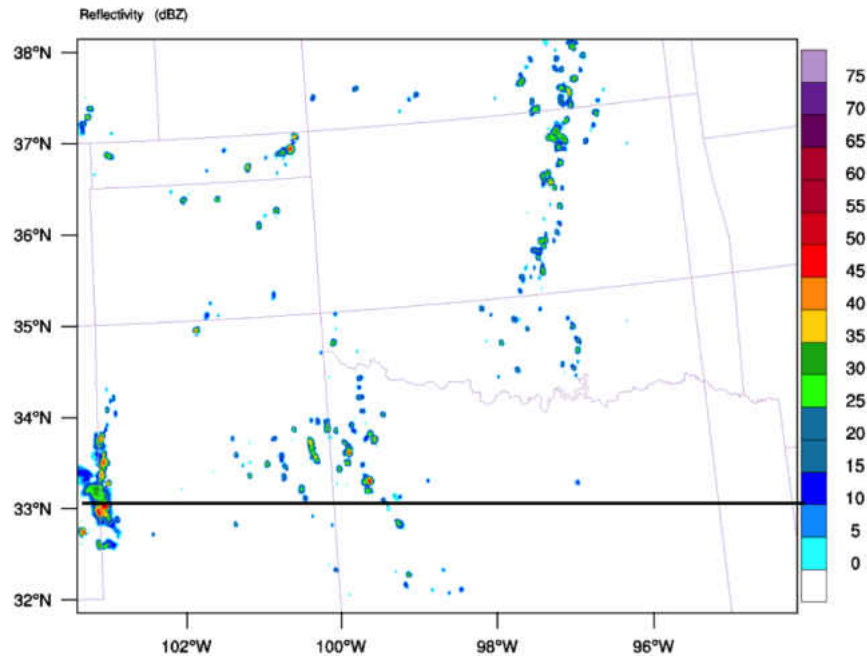
Fig. 19. Model derived radar reflectivity in the analysis domain, for an example QISC example case from May. In black, the line represents the plane on which a vertical cross section was taken. Case analyzed was 19 May 2007 at 2200Z.
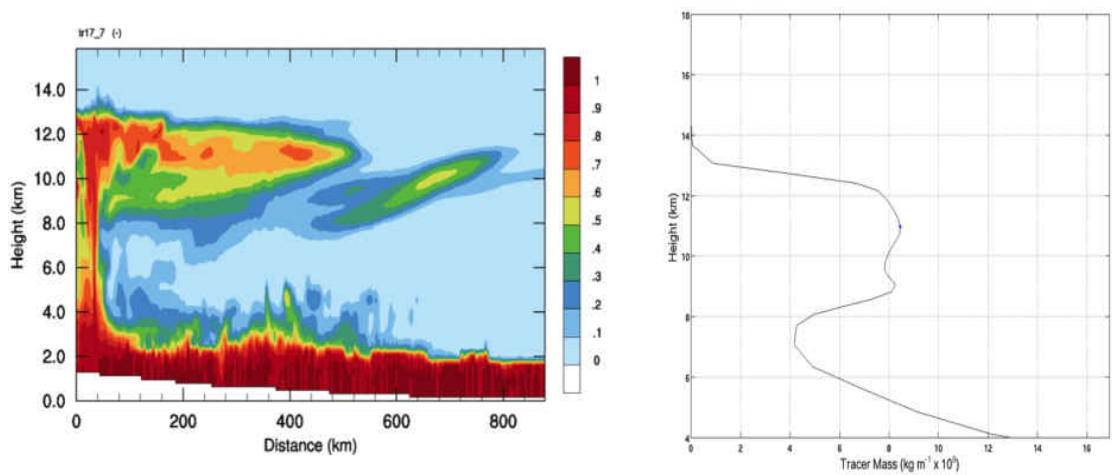
Fig. 20. A) vertical cross-section through an example May QISC storm of tracer concentration, analyzed at 2200Z on 19 May 2007, and b) the vertical profile of tracer mass for the domain at the time of the storm. The determined LMD is shown in b) by a blue asterisk.
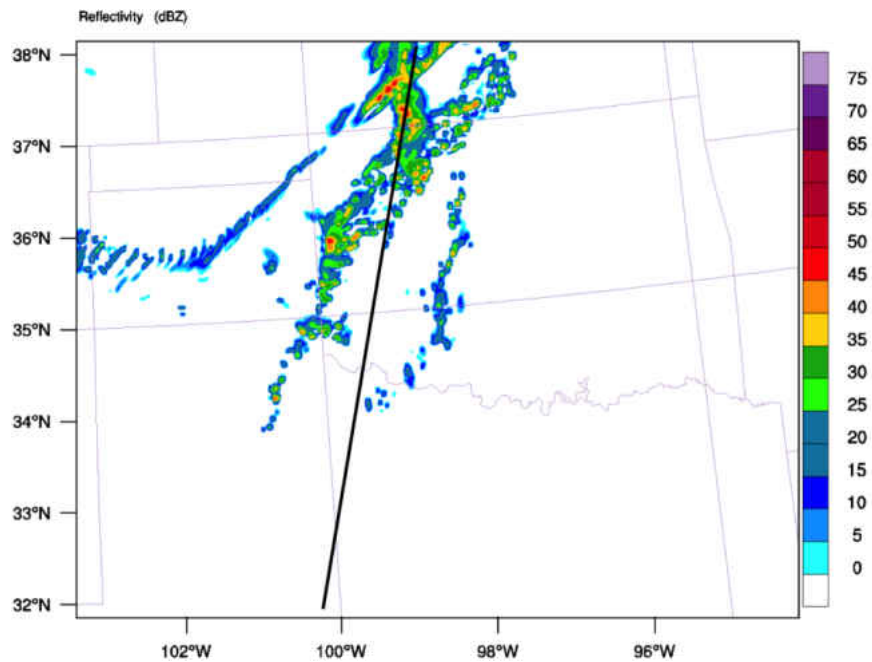
Fig. 21. As in Fig. 19, for an example MCS case from May. The case analyzed was on 15 May 2007 at 1100 Z.
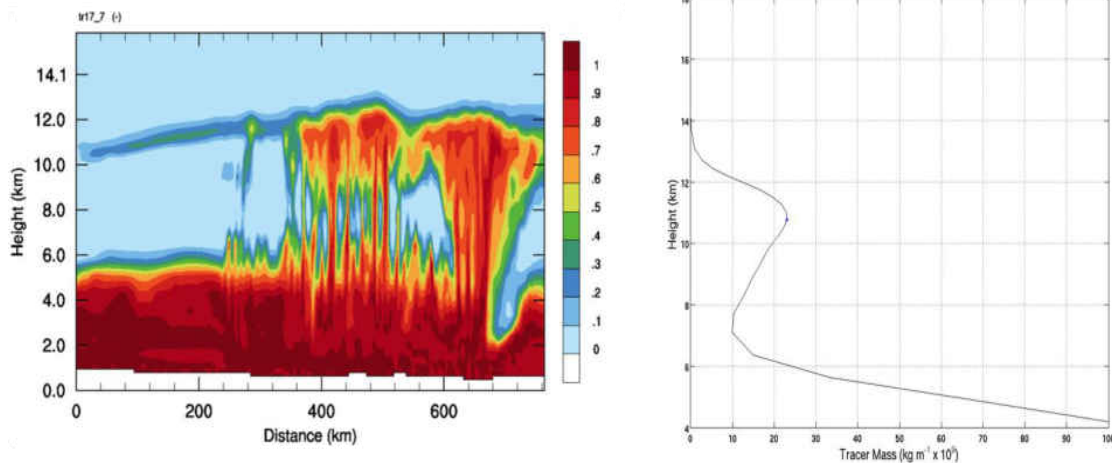
Fig. 22. As in Fig. 20, for an example MCS case from May, which was analyzed at 1100Z on 15 May 2007.

In contrast, estimates of the regional transport of mass to the upper troposphere for the QISC and MCS regimes (Fig. 18) are different, as the mean values (1.79×10^{11} kg m^{-1} and 3.21×10^{11} kg m^{-1}, respectively) and median values (1.05×10^{11} kg m^{-1} and 2.70×10^{11} kg m^{-1}, respectively) indicate that greater transport occurs with the MCS class. The profiles (right panels) of Figures 20 and 22 support this as well; as the total transport from the MCS was 3.24×10^{11} kg m^{-1} (Fig. 22) and that from the QISC (Fig. 20) was less than half of that (1.56×10^{11} kg m^{-1}). A paired t-test was used to evaluate the statistical significance of these differences. Any outliers in the data (shown as red plus signs in Figs. 17 and 18) were removed before calculation of this t-test to ensure that the distribution of the data is closer to normal. A p-value is calculated for this t-test, and is the probability that two means (from two datasets) are from the same set of data, which is the null hypothesis for this test. At the 95% confidence level (p = 0.05), a value smaller then the critical value is a statistically significant finding, and rejects the null hypothesis. A result greater than the critical value means that the null hypothesis cannot be rejected,

and more testing should be done to determine whether or not the values indeed come from the same dataset or not. The difference between the mean MCS and QISC LMD altitudes were not statistically significant, with a p-value for the test being 0.5748 at the 95% confidence level. In contrast, differences in the estimated transport magnitudes were statistically significant, as the p-value for the test was 4.2591×10^{-6} (> 99% confidence).
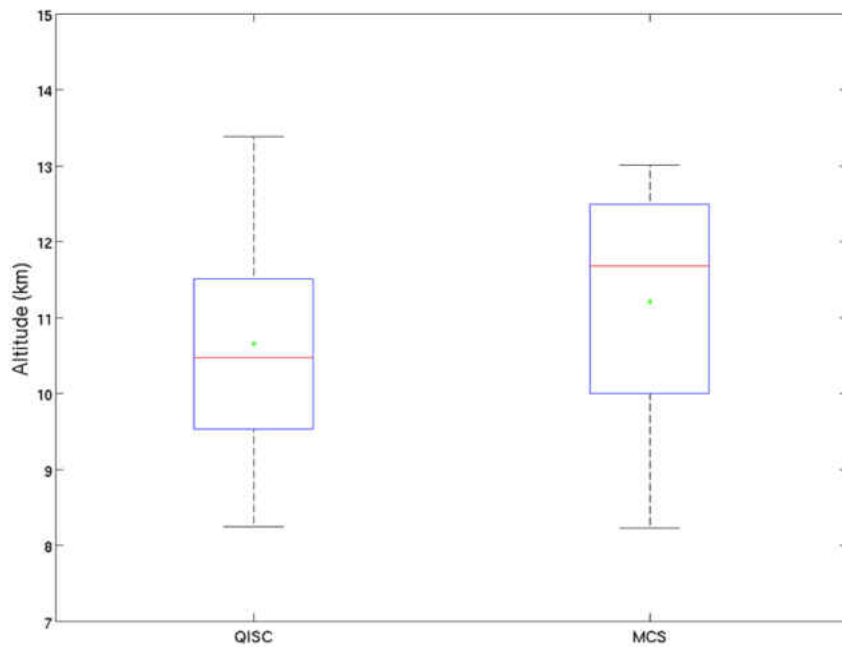
Fig. 23. As in Fig. 17, for July.
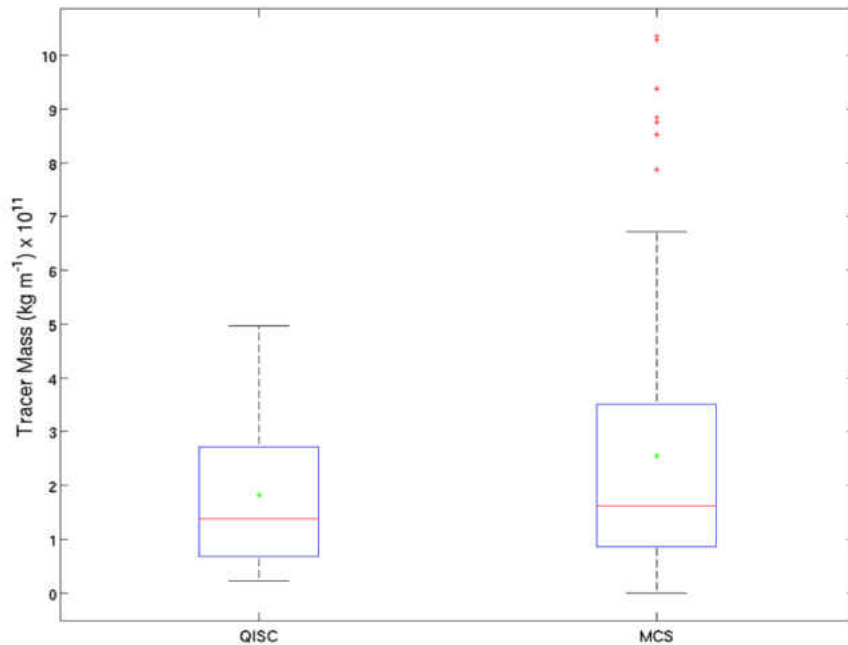
Fig. 24. As in Fig. 18, for July.

Figures 23 and 24 show the LMD and mass transport magnitude distributions for
each storm regime in July. The altitudes of the mean (11.21 km for MCS and 10.65 km
for QISC) and median (10.47 km for QISC and 11.67 km for MCS) LMDs were higher
for the MCS than the QISC during July (Fig. 23). These differences were statistically
significant at the 95% confidence level (p-value 0.0352). It is noted that the QISC
regime did have several instances with higher LMDs than contained within the MCS
distribution (vertical dashed lines). Examples for July are shown in Figures 25-28. The
example MCS case (Fig. 28) has a higher detrainment envelope (10 km to 14 km) than
the example QISC case (Fig. 26, 8 km to 11 km), which is consistent with the differences
presented in Fig. 23. The profiles (right panels Figs. 26, 28) show that the LMDs of the
two systems are very different (10.76 km for QISC and 12.74 km for MCS).

70
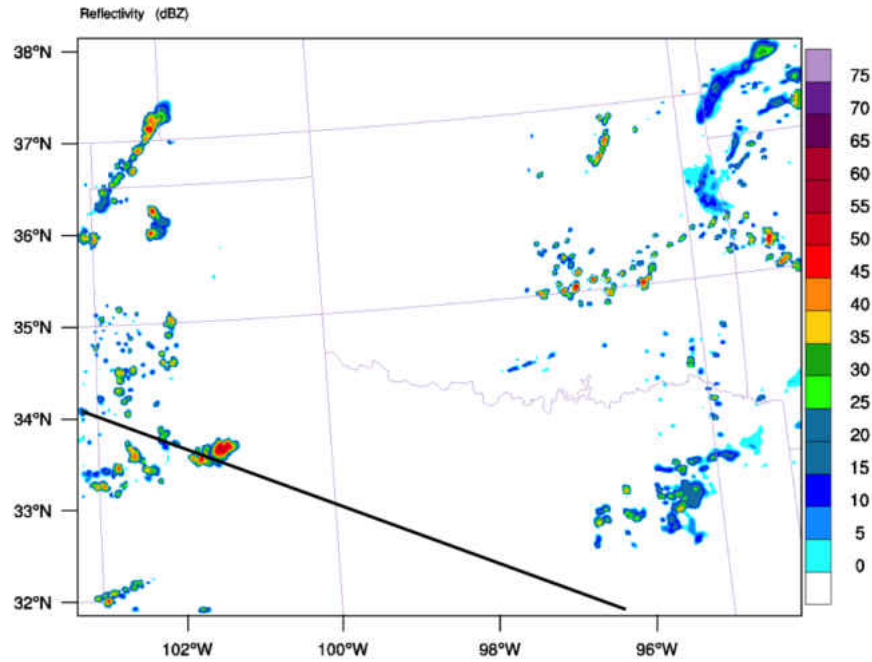
Fig. 25. As in Fig. 19, for an example QISC case from July. This case was on 10 July 2007 at 2000Z.
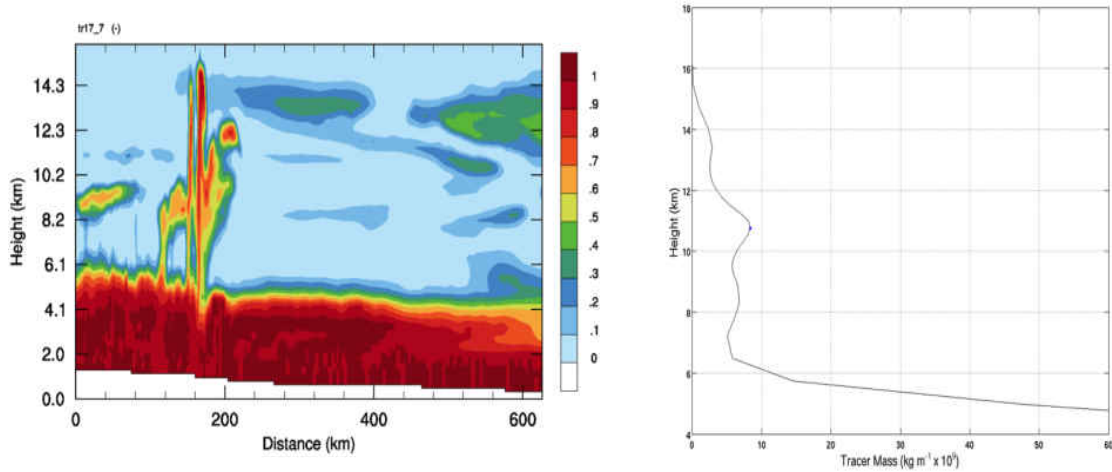
Fig. 26. A) vertical cross-section through an example July QISC storm of tracer concentration, analyzed at 2000Z on 10 July 2007, and b) the vertical profile of tracer mass for the domain at the time of the storm. The determined LMD is shown in b) by a blue asterisk.

71
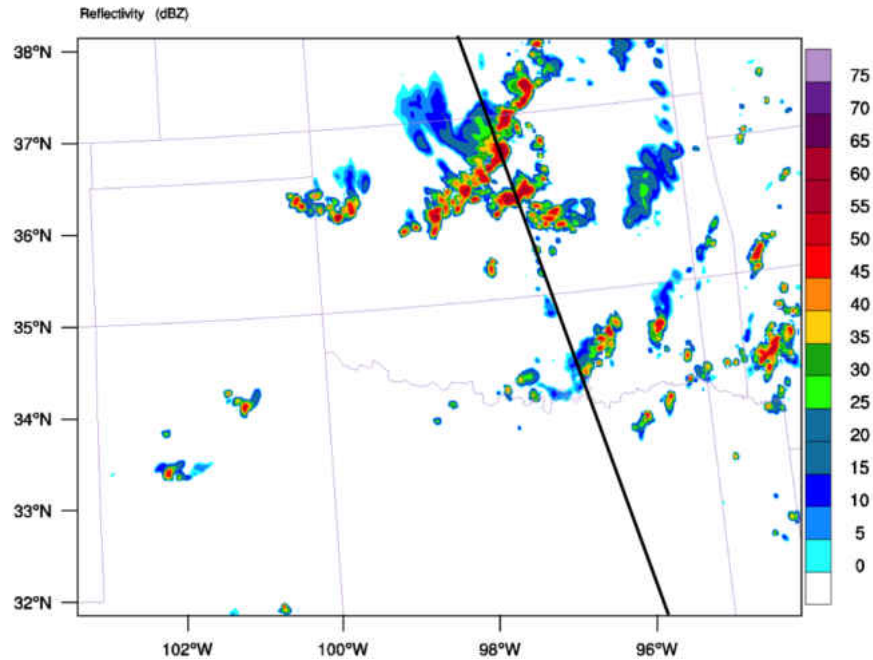
Fig. 27. As in Fig. 19, for an example MCS case from July. This case was on 10 July 2007 at 0000Z.
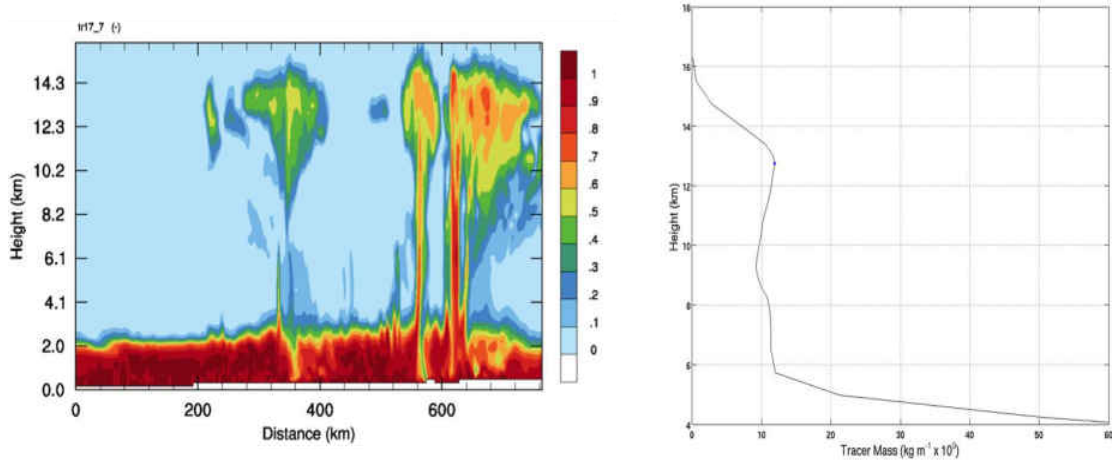
Fig. 28. As in Fig. 27, for an example July QISC, which was analyzed at 0000Z on 10 July 2007.

The mean magnitudes of mass transport for the QISC (1.81×10^{11} kg m^{-1}) and MCS (2.54×10^{11} kg m^{-1}), and the medians (1.37×10^{11} kg m^{-1} and 1.62×10^{11} kg m^{-1}, respectively), were similar (Fig. 24) and not statistically significant at the 95%

confidence level (p-value 0.3600). Profiles from the representative cases (Figs. 26, 28) also support this, as the transport totals for the two storms were 1.27 x 10^{11} kg m^{-1} for the QISC storm and 1.72 x 10^{11} kg m^{-1} for the MCS storm.

In summary, the convection in the QISC and MCS regimes transported mass to the same altitude (LMD) in May, but in July, the convection in the MCS regime transported to a higher altitude than convection in the QISC regime. In contrast, the amount of mass transported was larger in the MCS regime than in the QISC regime in May, but equal for the two regimes in July. To better understand these results, the distribution of the magnitude of mass transported *per storm* (instead of over all storms) and the LMD *relative to the tropopause* (instead of raw altitude) are analyzed. These helps remove variability associated with different storm counts or different synoptic environments, and provide information regarding the transport capabilities of individual storms.

First, the mass of tracer transported to the UTLS *per storm* is considered. As stated in the methodology (Chap. 3), this involved "normalizing" the total transported mass each hour by the number of objects in the domain that were identified as being deeply convective. Figures 29 and 30 show the distribution of this estimated mass. For May (Fig. 29), there is a difference in the mean (1.04 x 10^{11} kg m^{-1} for the QISC and 2.30 x 10^{11} kg m^{-1} for the MCS) and median (0.77 x 10^{11} kg m^{-1} for QISC and 1.98 x 10^{11} kg m^{-1} for MCS) values. The difference in the mean value was determined to be statistically significant (p-value of 2.062 x 10^{-4}, > 99% confidence). There are also differences between the July QISC and MCS values (Fig. 30), as the means (0.75 x 10^{11} kg m^{-1} and 1.58 x 10^{11} kg m^{-1}, respectively) and medians (0.72 x 10^{11} kg m^{-1} and 1.15 x 10^{11} kg m^{-1},

respectively) support the difference in the mean value being statistically significant (p-value of 2.498 x 10^{-4}, > 99% confidence).
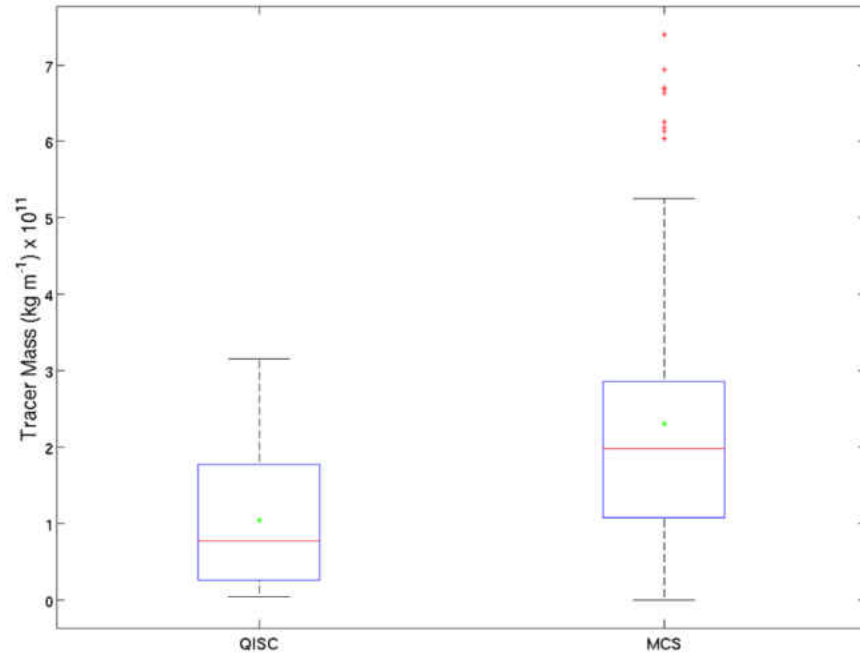
Fig. 29. Distribution of the estimated magnitude of deep convective transport normalized by the number of deeply convective objects, for May.
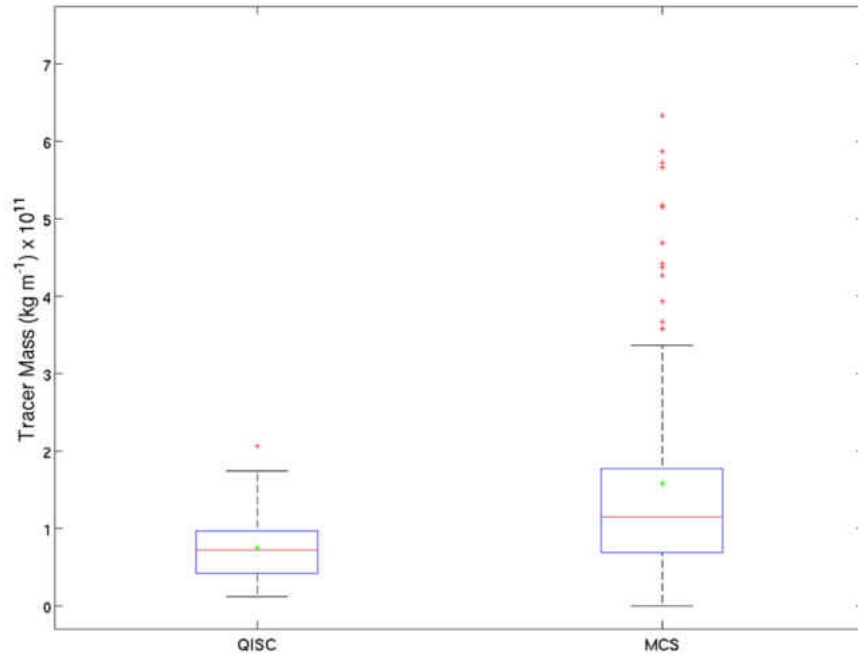
Fig. 30. As in Fig. 29, for July.

As the majority of boundary layer mass is transported in the cores of deep updrafts (e.g. Mullendore et al. 2005), the amount of deep convection in the domain at a given time is expected to relate to the amount of mass transported to the UTLS region. As such, Figures 31 and 32 show the distribution for each month of the areal coverage of deep convection. Figure 31 shows the differences between the QISC and MCS mean (see Table 6; 50.79 km^2 and 151.6 km^2, respectively) and median (16 km^2 and 92 km^2, respectively) values. The difference in the mean value between the two regimes was calculated to be statistically significant (p-value of 0.0011, 99% confidence). Similarly for July (Fig. 32), the differences in the mean (see Table 7; 42.22 km^2 for QISC and 112.8 km^2 for MCS) and median (2 km^2 for QISC and 32 km^2 for MCS) values were statistically significant (p-value of 6.699 x 10^{-4}, > 99% confidence).
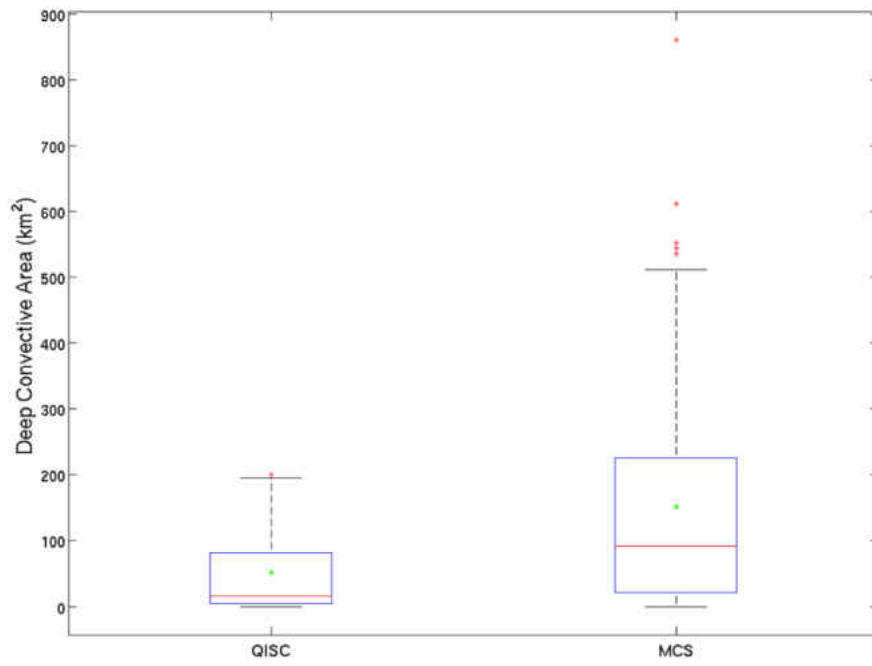
Fig. 31. Distribution of the areal coverage in the domain by deep convection for May.
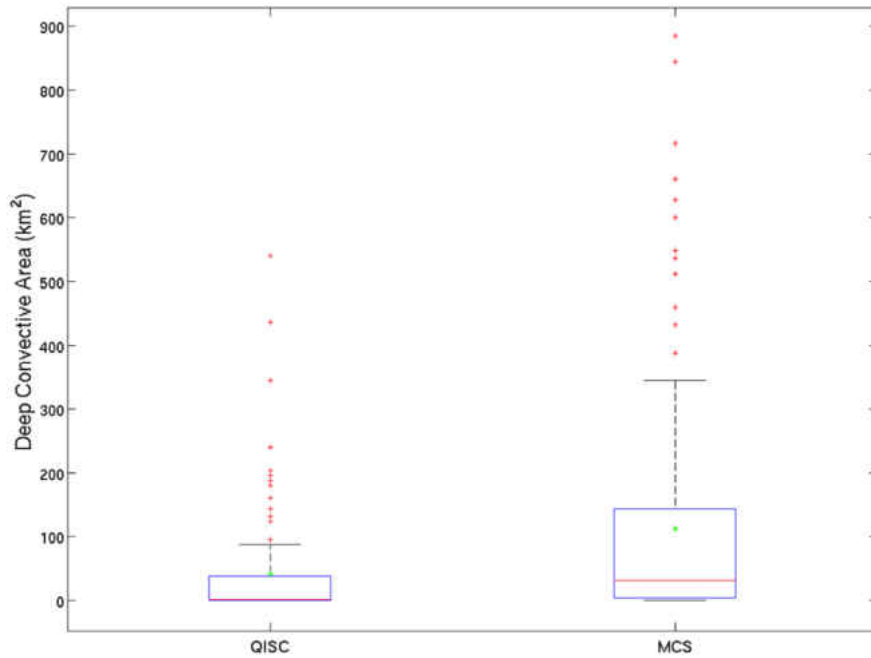
Fig. 32. As in Fig. 31, for July.

Further investigation into the depth of the transport for each regime is performed similarly to Mullendore et al. (2009, 2013), who compared the LMD altitude for an MCS storm, a multicell storm and a supercell storm (the multicell and supercell storms would be in the QISC class for this study), to the height of the level of neutral buoyancy (LNB). In this study, the tropopause height, as determined with the NARR 3-hourly dataset, is used instead of a direct calculation of the LNB. The LMD is determined using the same method as mentioned above for the altitude calculations (see Figs. 17, 23), except that the altitude is now shifted to be relative to the tropopause height (Figs. 33, 34).
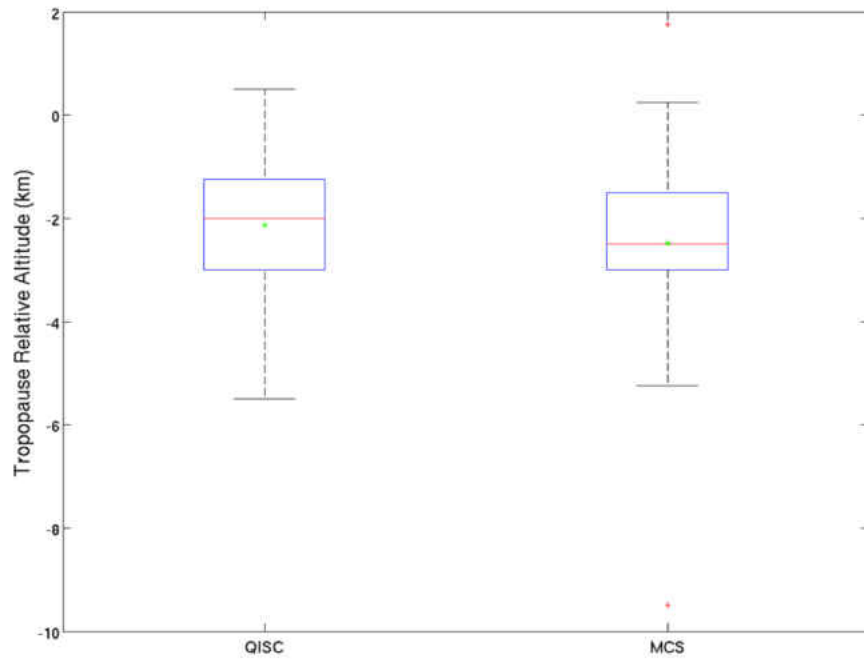
Fig. 33. Distribution of the tropopause-relative LMD for May.
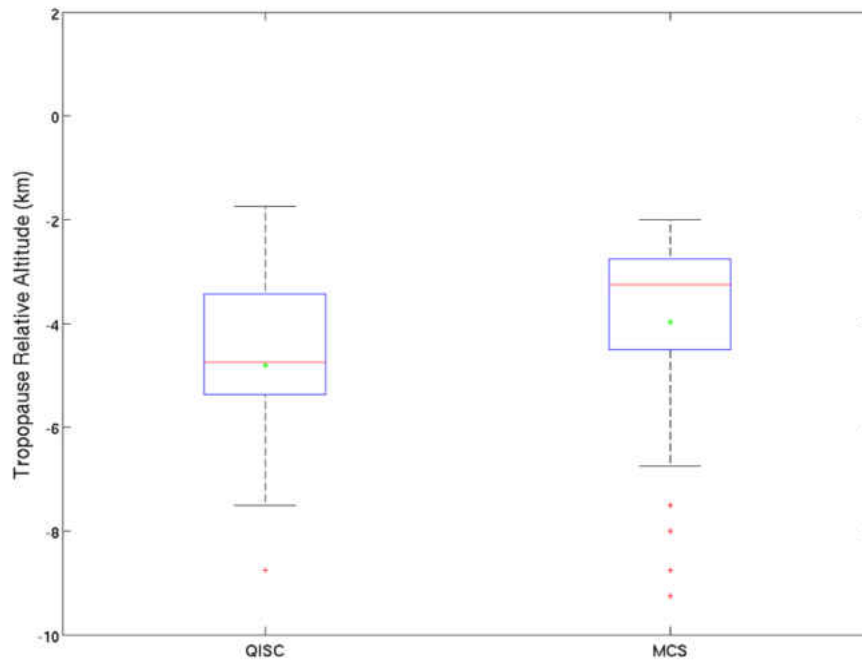
Fig. 34. As in Fig. 33, except for July.

The results for this investigation agree with the results presented previously for

the altitude of the LMD (Figs. 17, 23) in terms of the differences between the two

analyzed regimes. In May (Fig. 33), the mean values of the tropopause-relative LMD for

the QISC regime (-2.13 km) and the MCS regime (-2.20 km), are very similar, as are the

median values (-2 km for QISC and -2.25 km for MCS).   The results of performing the

paired t-test on this data showed that indeed the differences were not statistically

significant (p-value 0.6996, 30% confidence). In contrast, in July the MCS regime

transported mass to a higher tropopause-relative altitude than the QISC regime (Fig. 34)

with the differences in the mean (-4.81 km for QISC and -3.97 km for MCS) and median

values (-4.75 km for QISC and -3.25 km for MCS). The difference in the mean value

found was determined to be statistically significant (p-value of 4.07 x 10^{-6}, > 99% confidence).

<p style="text-align:center">Discussion</p>

The results of this study show that domain-wide transport magnitude for different storm regimes may look different (May; Fig. 18) or similar (July; Fig. 24), however the transport per storm gave a more consistent picture over the two months (Figs. 29, 30) in that there were significant differences in the mean value for both months. For July (Table 7), the number of hours for which QISC storms were dominant (92) was relatively similar to the number of hours for which MCS storms were dominant (138). In May (Table 6) this is much different, though, as the QISC class was dominant only 38 hours relative to 183 hours for the MCS class. It was found that the MCS storms individually transport significantly more mass to the UTLS region than do the QISC storms for both May (Fig. 29; p-value of 2.062 x 10^{-4}, > 99% confidence) and July (Fig. 30; p-value of 2.498 x 10^{-4}, > 99% confidence). These results demonstrate that for deep convective transport to be correctly represented in simulations that do not resolve individual storms, e.g. global transport models, not only the amount of convective activity, but also the *type* of convective activity, needs to be resolved.

The areal coverage of deep convection in May (Fig. 31) and July (Fig. 32) were significantly different [p-value of 0.0011 for May (99% confidence) and p-value of 6.699 x 10^{-4} for July (> 99% confidence)]. The amount of deep convection in the domain at a given time relates to the amount of mass transported to the UTLS region, because it indicates the relative updraft coverage for each regime. Figure 35 shows vertical cross

sections of tracer concentration for MCS and QISC systems that occurred in May and July. Both MCS systems have wider horizontal areas of strong tracer concentrations (i.e., tracer concentrations greater than ~0.8 g kg^{-1}; Fig. 35 a,c). These wider zones of high tracer concentration suggest wider updrafts, which would in turn lead to more transport of undiluted tracer from the boundary layer to the UTLS region. Conversely, the QISC regime shows storms having narrower updrafts (Fig. 35 b,d), leading to less undiluted transport.
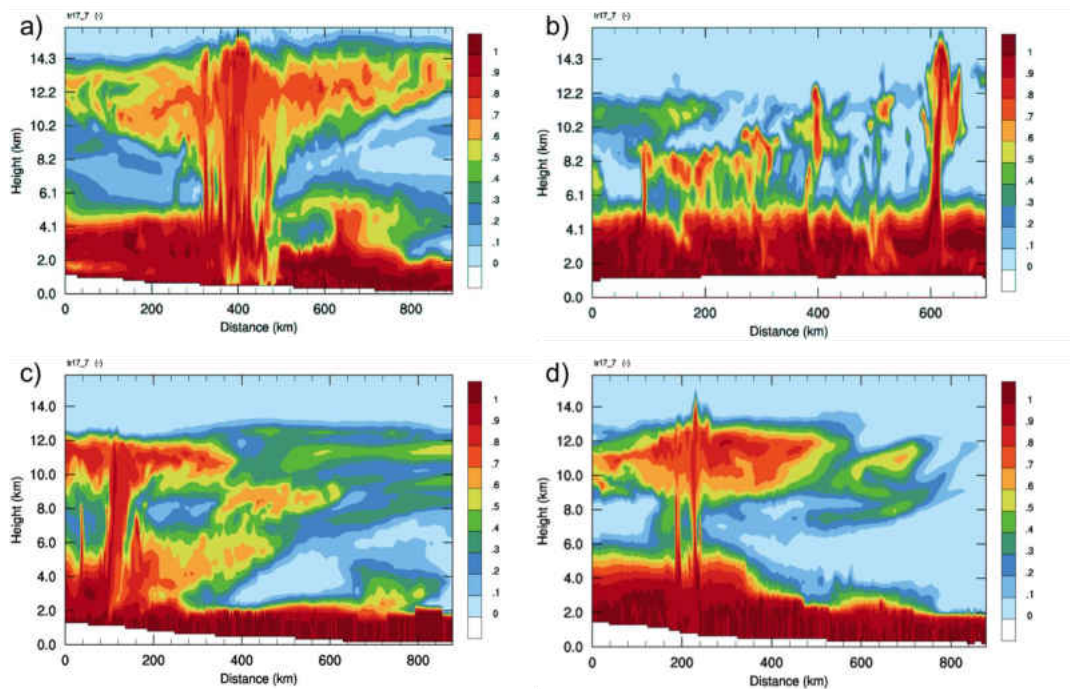
Fig. 35. Vertical cross sections of tracer concentration. A) An MCS from 13 July 2007 at 0600Z. B) A QISC from 10 July 2007 at 2300Z. C) An MCS from 18 May 2007 at 1800Z. D) A QISC from 20 May 2007 at 2100Z.

It was also found that the altitude to which the storms transport mass compared to that of the tropopause height was similar in May (Fig. 33, p-value of 0.6996 which is 30% confidence) and significantly different in July (Fig. 34, p-value of 4.07×10^{-6} which is > 99% confidence). These results are consistent with the results on the domain-wide

scale. It was found that there were instances in May where the altitude of the LMD relative to the tropopause was > 0, however in July the maximum values approached only ~ -2 km. The cause of these differences may be due to the convective environment, and, subsequently, the overall organization of storms. The presence, or lack thereof, of supercells in the domain may also cause this, as supercells are more likely during the month of May than in July.

The results presented in this study are consistent with those from previous studies such as Mullendore et al. (2005) and Cotton et al. (1995), who found that transport of chemical constituents in deep convection could vary greatly with storm type. Many previous studies, however, have evaluated deep convective transport using a single type of convection (Pickering et al. 1992; Thompson et al. 1994; Stenchikov et al. 1996; Hintsa et al. 1998; Barth et al. 2007; Halland et al. 2009). Studies that focused on a single storm, or type of storm, cannot provide a good understanding of relative contributions of different storm regimes to the overall budget of transport of boundary layer air to the UTLS. This is where the current study differs from previous research in that this is the first study where an objective classification scheme is actively applied to seasonally simulated storms such that transport characteristics can be analyzed for each regime, specifically, the characteristics of two dynamically important regimes, quasi-isolated strong convection and mesoscale convective systems.

The results presented herein provide a basis for future studies that examine the contributions of different storm regimes to the transport budget on a larger time scale. Future studies will be necessary in order to strengthen the findings of this study. For example, the current study is only run over a span of 4 total weeks. Simulating the entire

convective season (April-August) over many years, including both wet and dry years, would provide more information regarding differences that exist between storm regimes. This study also lays the groundwork for sensitivity studies regarding the parameters that most affect storm classification. One of the main challenges is representing cases accurately that are near the lateral model domain boundaries. For example, the MCS shown in Figure 35c was a case wherein only part of the storm was in the analysis domain. With the estimated "anvil" area not capturing the whole storm, the total transport for that MCS was lower (2.42×10^{11} kg m^{-1}) than for the example QISC case from May (3.15×10^{11} kg m^{-1}; Fig. 35d).

Another challenge encountered in this study is regimes are not "tracked" in time. An analyzed QISC that becomes a large, long-lived MCS two hours after the analysis is treated as a QISC, and not as a developing MCS. This is the same as an MCS that eventually becomes WC within a couple hours of the MCS being analyzed as such it is not classified as a decaying MCS. Tracking regime evolution would certainly change the results, as only mature storms of each regime are analyzed and should accentuate differences in the transport characteristics between the different regimes. Examination of the tunable parameters of the classification scheme in the current study identified some of this variability (Tables 4 and 5, Chap. 3).

One parameter that could be studied is the amount of high reflectivity (> 40 dBZ threshold) in an object that is required for it to qualify as either an MCS or QISC. The reason for this is because, in a large system (i.e. MCS), having only a few columns of deep convection in the system may not actually be representative of the presence of a deep updraft or strong concentration of hydrometeors. Instead, future work should

include a method of determining strong convection as a percentage of the total storm area containing reflectivities > 40 dBZ. Removing cases in which such a condition is not met should cause both LMD and transport magnitude means to increase, since these cases are most likely more representative of WC than an MCS, and would be causing the mean values of LMD and transport magnitude to be lower than they would if represented correctly.

Another methodology that could change is within the classification scheme. Currently, supercells are classified within the QISC regime. As discussed in the background, supercells are very dynamically different than the other storms within this regime (single cells and multicells). The individual environments in which supercells are favored are also very different. As such, future work should objectively determine if a QISC storm is a supercell or not, and if so, separate it as its own classification, leaving just single cells and multicells in the QISC class. It is expected that such a separation would provide more information on the differences between MCSs and QISCs, MCSs and supercells, and, perhaps even more importantly as support of this study, between supercells and QISCs.

It is acknowledged that regional differences factor into seasonal convective environments, and thus seasonally preferred convective mode. Future work should analyze the transport characteristics in different regions during the convective season, such as was done during the Deep Convective Clouds and Chemistry (DC3) field campaign of 2012, which was done over Oklahoma/northern Texas, Colorado, and northern Alabama. An example of the differences in region that would affect results of analyzed transport characteristics is the southeastern U.S. (including northern Alabama).

This region is less likely to have supercells than Oklahoma (though there are still a few events yearly with strong supercells). In the convective season studied here (May and July) both months exhibit characteristics of subtropical warm-sector convection. The predominant storm type is single cell pulse-like convection and multicellular convection (QISC). MCSs are also possible when the synoptic forcing (fronts) move through the area, but are much less common than they are in other regions.

CHAPTER V

CONCLUSIONS

The purpose of this study is to examine the differences in deep convective

transport characteristics between different thunderstorm regimes. An objective

classification scheme based loosely on that by Schoen and Ashley (2011) was utilized to

classify thunderstorms that were simulated by the WRF-CHEM model, version 3.2.1. A

completely passive tracer was initialized solely and uniformly in the boundary layer and

then allowed to be advected by both large-scale and storm-scale motions. Properties of

the transport of those tracers, mainly the altitude to which the tracer was transported and

the estimated magnitude of the mass of the tracer transported, were analyzed for the

quasi-isolated strong convection (QISC) and mesoscale convective system (MCS)

regimes. The fundamental result is that, per storm complex, the MCS class of storms

transported more mass from the boundary layer to the upper troposphere than the QISC

class of storms. However, while domain wide the MCS class transported more mass than

the QISC class in May, their transport was nearly equal in July. The altitudes to which

mass was transported in both the MCS and QISC regimes in terms of the LMD and the

LMD relative to the tropopause height were similar for the month of May but

significantly higher for July.

The results of this study are summarized as:

1) For May, the MCS regime transported approximately 1.8 times more tracer mass to the UTLS region than the QISC regime. In July, although the MCS regime transported 1.4 times more tracer mass to the UTLS than the QISC regime, the difference in magnitude was not statistically significant.

2) The magnitude of mass transport *per storm* revealed that MCSs transported more mass per storm than did QISC systems for both May and July. For May, the MCS regime transported 2.2 times the amount of tracer mass *per storm* than did the QISC regime. In July, this difference was only slightly smaller, with the MCS regime transporting 2.1 times the amount of mass *per storm* than did the QISC regime.

3) The MCS regime and QISC regime transported mass to relatively similar altitudes for May. The mean value for the MCS regime was only 150 m higher than that for the QISC regime, which was found to not be a statistically significant difference. In contrast, the difference in the mean value for the LMD altitude between the MCS regime and QISC regime was 560 m, which was a significant difference.

4) As a comparison to (3), the LMD altitude relative to the tropopause height was calculated. In May, the difference between the mean value for the MCS regime and QISC regime was 70 m, which was not a significant difference. In contrast, the difference in the mean values for July was 840 m, which was a significant finding.

5) The amount of the domain covered by deep convection when a regime was dominant was also calculated. It was determined that, for May, the MCS regime

had 3 times more deeply convective area than the QISC regime. In July, the MCS

regime had 2.7 times the amount of QISC deep convection.

This study has shown that the use of objective classification schemes in studies of mass

transport is important. For studies that do not resolve individual storms, such as global

transport models, this study has shown that not only is the amount of convective activity

important for analyzing difference in tracer transport characteristics, but resolving the

type of convection is crucial to understanding the variability associated with transport due

to different convective regimes. By being the first study to actively apply an objective

classification scheme to seasonal simulations, it has shown that the two dynamically

important regimes studied (QISC and MCS regimes) cannot be assumed to exhibit similar

properties of transport. To accurately estimate the overall transport budget, such methods

of classification are necessary.

REFERENCES

Aligo, E., W. Gallus Jr., and M. Segal, 2009: On the impact of WRF model vertical grid resolution on Midwest summer rainfall forecasts. *Wea. Forecasting*, **24**, 575–594.

Arakawa, Akio, 2004: The Cumulus Parameterization Problem: Past, Present, and Future. *J.Climate*, **17**, 2493–2525.

Barth, M.C., and Coauthors, 2007: Cloud-scale model intercomparison of chemical constituent transport in deep convection. *Atmos. Chem. Phys.,* **7**, 4709-4731.

Bechtold, P., E. Bazile, F. Guichard, P. Mascart, and E. Richard, 2001: A mass-flux convection scheme for regional and global models. *Q. J. R. Meteorol. Soc*., **127**, 869–886.

Bechtold, P., J. P. Chaboureau, A. Beljaars, A. K. Betts, M. Köhler, M. Miller, and J. L. Redelsperger, 2004: The simulation of the diurnal cycle of convective precipitation over land in a global model. *Q. J. R. Meteorol. Soc*., **130**, 3119–3137.

Bélair, S., and J. Mailhot, 2001: Impact of horizontal resolution on the numerical simulation of a midlatitude squall line: Implicit versus explicit condensation. *Mon. Wea. Rev.*, **129**, 2362-2376.

Betts, A. K., and M. J. Miller, 1993: The Betts–Miller scheme. *The Representation of Cumulus Convection in Numerical Models, Meteor.Monogr.,*No. 46, Amer. Meteor. Soc., 107–121.

Bluestein, H. B., and M. H. Jain, 1985: Formation of mesoscale lines of precipitation: Severe squall lines in Oklahoma during the spring. *J. Atmos. Sci.,* **42**, 1711-1732.

Brooks, H. E., and R. B. Wilhelmson, 1993: Hodograph curvature and updraft intensity in numerically modeled supercells. *J. Atmos. Sci.*, **50**, 1824-1833.

Brown, B. G., R. Bullock, J. Halley Gotway, D. Ahijevych, C. Davis, E. Gilleland, and L. Holland, 2007: Application of the MODE object-based verification tool for the evaluation of model precipitation fields. *AMS 22nd Conference on Weather Analysis and Forecasting and 18th Conference on Numerical Weather Prediction*, 25-29 June, Park City, Utah, American Meteorological Society (Boston), Available at http://ams.confex.com/ams/pdfpapers/124856.pdf.

Bryan, G. H., J. C. Wyngaard, and J. M. Fritsch, 2003: Resolution requirements for the simulation of deep moist convection. *Mon. Wea. Rev.*, **131**, 2394-2416.

Chatfield, R. B., and P. J. Crutzen, 1984: Sulfur dioxide in remote oceanic air: Cloud transport and reactive precursors. *J. Geophys. Res.*, **89**, 7111-7132.

Clark, A. J., W. A. Gallus Jr., and T. –C. Chen, 2007: Comparison of the diurnal precipitation cycle in convection-resolving and non-convection-resolving mesoscale models. *Mon.Wea.Rev.*, **135**, 3456-3473.

Cohen, C., 2000: A Quantitative investigation of entrainment and detrainment in numerically simulated cumulonimbus clouds. *J. Atmos. Sci.*, **57**, 1657-1674.

Collins, W. J., D. S. Stevenson, C. E. Johnson, and R. G. Derwent, 1999: Role of convection in determining the budget of odd hydrogen in the upper troposphere. *J. Geophys. Res.*, **104**, 26927-26941.

Cotton, W. R., G. D. Alexander, R. Hertenstein, R. L. Walko, R. L. McAnelly, and M. Nicholls, 1995: Cloud venting- A Review and some new global annual estimates. *Earth-Science Reviews*, **39**, 169-206.

Davis, C. A., B. G. Brown, and R. G. Bullock, 2006a: Object-based verification of precipitation forecasts, Part I: Methodology and application to mesoscale rain areas. *Mon. Wea. Rev.*, **134**, 1772-1784.

Davis, C. A., B. G. Brown, and R. G. Bullock, 2006b: Object-based verification of precipitation forecasts, Part II: Application to convective rain systems. *Mon. Wea. Rev.*, **134**, 1785-1795.

Del Genio, Anthony D., Jingbo Wu, Yonghua Chen, 2012: Characteristics of Mesoscale Organization in WRF Simulations of Convection during TWP-ICE. *J. Climate*, **25**, 5666–5688.

Dickerson, R. R., and Coauthors, 1987: Thunderstorms: An important mechanism in the transport of air pollutants. *Science*, **235**, 460-465.

Doherty, R. M., D. S. Stevenson, W. J. Collins, and M. G. Sanderson, 2005: Influence of convective transport on tropospheric ozone and its precursors in a chemistry-climate model. *Atmos. Chem. Phys.*, **5**, 3205-3218.

Done, J., C. A. Davis, and M. L. Weisman, 2004: The next generation of NWP: explicit forecasts of convection using the weather research and forecasting (WRF) model. *Atmos. Sci. Let.*, **5**, 110-117.

Doswell, C. A., H. E. Brooks, and R. A. Maddox, 1996: Flash flood forecasting: An ingredients-based methodology. *Wea. Forecasting*, **11**, 560-581.

Emanuel, K. A. and M. Zivkovic-Rothman, 1999: Development and evaluation of a convection scheme for use in climate models. *J. Atmos. Sci.*, **56**, 1766-1782.

Emmons, L. K., and Coauthors, 2010: Description and evaluation of the Model for Ozone and Related chemical Tracers, version 4 (MOZART-4). *Geosci. Model Dev.*, **3**, 43-67.

Fischer, H., and Coauthors, 2003: Deep convective injection of boundary layer air into the lowermost stratosphere at midlatitudes. *Atmos. Chem. Phys.*, **3**, 739-745.

Gagne, D. J., A. McGovern, and J. Brotzge, 2009: Classification of convective areas using decision trees. *J. Atmos. Oceanic Technol.*, **26**, 1341-1353.

Gallus, W. A., J. Correia Jr., and I. Jankov, 2005: The 4 June 1999 derecho event: A particularly difficult challenge for numerical weather prediction. *Wea. Forecasting*, **20**, 705-728.

Gallus, W. A., N. A. Snook, and E. V. Johnson, 2008: Spring and summer severe weather reports over the Midwest as a function of convective mode: A preliminary study. *Wea. Forecasting*, **23**, 101-113.

Grams, J. S., W. A. Gallus, S. E. Koch, L. S. Wharton, A. Loughe, and E. E. Ebert, 2006: The use of a modified Ebert-McBride technique to evaluate mesoscale model QPF as a function of convective system morphology during IHOP 2002. *Wea. Forecasting*, **21**, 288-306.

Grell, G. A., 1993: Prognostic evaluation of assumptions used by cumulus parameterizations. *Mon. Wea. Rev.*, **121**, 764-787.

Grell, G. A., and D. Dévényi, 2002: A generalized approach to parameterizing convection combining ensemble and data assimilation techniques. *Geophys. Res. Lett.*, **29**, 1693.

Grell, G. A., R. Knoche, S. E. Peckham, and S. A. McKeen, 2004: Online versus offline air quality modeling on cloud-resolving scales. *Geophys. Res. Lett.*, **31**, L16117.

Grell, G. A., S. E. Peckham, R. Schmitz, S. A. McKeen, G. Frost, W. C. Skamarock, and B. Eder, 2005: Fully coupled "online" chemistry within the WRF model. *Atmos. Environ.*, **39**, 6957-6975.

Hack, J. J., 1994: Parameterization of moist convection in the National Center for Atmospheric Research community climate model (CCM2). *J. Geophys. Res.*, **99**, 5551-5568.

Halland, J. J., H. E. Fuelberg, K. E. Pickering, and M. Luo, 2009: Identifying convective transport of carbon monoxide by comparing remotely sensed observations from TES with cloud modeling simulations. *Atmos. Chem. Phys.*, **9**, 4279-4294.

Hauf, T., P. Schulte, R. Alheit, and H. Schlager, 1995: Rapid vertical trace gas transport by an isolated midlatitude thunderstorm. *J. Geophys. Res.*, **100**, 22,957-22,970.

Hegglin, M. I., and Coauthors, 2004: Tracing troposphere-to-stratosphere transport above a mid-latitude deep convective system. *Atmos. Chem. Phys.*, **4**, 741-756.

Hintsa, E. J., and Coauthors, 1998: Troposphere-to-stratosphere transport in the lowermost stratosphere from measurements of H_2O, CO_2, N_2O, and O_3. *Geophys. Res. Let.*, **25**, 2655-2658.

Holton, J. R., P. H. Haynes, M. E. McIntyre, A. R. Douglass, R. B. Rood, and L. Pfister, 1995: Strstosphere-troposphere exchange. *Rev. Geophys.*, **33**, 403-439.

Hong, S.-Y., and Y. Noh, and J. Dudhia, 2006: A new vertical diffusion package with an explicit treatment of entrainment processes. *Mon. Wea. Rev*., **134**, 2318–2341.

Houze, R. A., Jr., 1993: *Cloud Dynamics*. Academic Press, San Diego, 573 pp.

Jacob, D.J., 1999: *Introduction to Atmospheric Chemistry*. Princeton University Press, 264 pp.

Janjić, Z. I., 1994: The step-mountain Eta coordinate model: Further developments of the convection, viscous sublayer, and turbulence closure schemes. *Mon. Wea. Rev.*, **122**, 927-945.

Janjić, Z. I., 2001: Nonsingular implementation of the Mellor-Yamada level 2.5 scheme in the NCEP Meso Model. NOAA/NWS/NCEP Office Note 437, 61 pp.

Jankov, I., W. A. Gallus Jr., M. Segal, B. Shaw, and S. E. Koch, 2005: The impact of different NWP model physical parameterizations and their interactions on warm season MCS rainfall. *Wea. Forecasting*, **20**, 1048-1060.

Jankov, I., and Coauthors, 2010: An evaluation of five WRF-ARW microphysics schemes using synthetic GOES imagery for an atmospheric river event affecting the California coast. *J. Hydrometeor*, doi:10.1175/2010JHM1282.1.

Kain, John S., J. Michael Fritsch, 1990: A One-Dimensional Entraining/Detraining Plume Model and Its Application in Convective Parameterization.*J. Atmos. Sci.*, **47**, 2784–2802.

Kain, J. S., and J. M. Fritsch, 1993: Convective parameterization for mesoscale models: The Kain-Fritsch scheme. *The Representation of Cumulus Convection in Numerical Models, Metoeor.Monogr.*, No. 46, Amer. Meteor. Soc., 165-170.

Kain, J. S., S. J. Weiss, M. E. Baldwin, G. W. Carbin, D. A. Bright, J. J. Levit, and J. A. Hart, 2005: Evaluating high-resolution configurations of the WRF model that are used to forecast severe convective weather: The 2005 SPC/NSSL Spring Program. Preprints, *21st Conf. on Weather Analysis and Forecasting and 17th Conf. on Numerical Weather Prediction*, Washington, DC, Amer. Meteor.Soc., 2A.5.[Available online at http://ams.confex.com/ams/pdfpapers/94843.pdf.]

Kessler, E., 1985: *Thunderstorm Morphology and Dynamics*. Univ. of Okla. Press, 432 pp.

Lawrence, M. G., R. von Kuhlmann, M. Salzmann, and P. J. Rasch, 2003b: The balance of effects of deep convective mixing on tropospheric ozone. *Geophys. Res. Lett.*, **30**, 1940.

Lawrence, M. G., and P. J. Rasch, 2005: Tracer transport in deep convective updrafts: Plume ensemble versus bulk formulations. *J. Atmos. Sci.*, **62**, 2880-2894.

Lawrence, M. G., and M. Salzmann, 2008: On interpreting studies of tracer transport by deep cumulus convection and its effects on atmospheric chemistry. *Atmos. Chem. Phys.*, **8**, 6037-6050.

Lelieveld, J. and P. J. Crutzen, 1994: Role of deep cloud convection in the ozone budget of the troposphere. *Science*, **264**, 1759-1761.

Levy, H., II, J. D. Mahlman, and W. J. Moxim, 1980: A stratospheric source of reactive nitrogen in the unpolluted troposphere. *Geophys Res. Lett.*, **7**, 441-444.

Lin, Y.-L., R. D. Farley, and H. D. Orville, 1983: Bulk parameterization of the snow field in a cloud model. *J. Climate Appl. Meteor.*, **22**, 1065-1092.

Liu, S. C., J. R. McAfee, and R. J. Cicerone, 1984: Radon-222 and tropospheric vertical transport. *J. Geophys. Res.*, **89**, 7291-7297.

Lu, R., C. Lin, R. Turco, and A. Arakawa, 2000: Cumulus transport of chemical tracers 1. Cloud-resolving model simulations.*J. Geophys. Res.*, **105**, 10,001-10,021.

Mahoney, K. M., and G. M. Lackmann, 2006: The sensitivity of numerical forecasts to convective parameterization: A case study of the 17 February 2004 East Coast cyclone. *Wea. Forecasting*, **21**, 465-488.

Mahowald, N. M., P. J. Rasch, and R. G. Prinn, 1995: Cumulus parameterizations in chemical transport models. *J. Geophys. Res.*, **100**, 26173-26189.

Mahowald, N. M., P. J. Rasch, B. E. Eaton, S. Whittlestome, and R. G. Prinn, 1997b: Transport of 222-Radon to the remote troposphere using the Modell of Atmospheric Transport and Chemistry and assimilated winds from ECMWF and the National Center for Environmental Prediction/NCAR. *J. Geophys. Res.*, **102**, 28139-28152.

Marshall, J. S., and W. McK. Palmer, 1948: The distribution of raindrops with size. *J. Meteor.*, **5**, 165-166.

Markowski, P., and Y. Richardson, 2010: Mesoscale meteorology in midlatitudes. Wiley-Blackwell, West Sussex, PO19 8SQ, United Kingdom, 407 pp.

Mesinger, F., and Coauthors, 2006: North American Regional Reanalysis. *Bull. Amer. Meteor. Soc.*, **87**, 343–360.

Moller, A. R., C. A. Doswell III, M. P. Foster, and G. R. Woodall, 1994: The operational recognition of supercell thunderstorm environments and storm structures. *Wea. Forecasting*, **9**, 327-347.

Morrison, H., J. A. Curry, and V.I. Khvorostyanov, 2005: A new double-moment microphysics parameterization for application in cloud and climate models. Part I: Description. *J. Atmos. Sci.*, **62**, 1665-1677.

Morrison, H., and J. O. Pinto, 2005: Mesoscale modeling of springtime arctic mixed-phase clouds using a new two-moment bulk microphysics scheme. *J. Atmos. Sci.*, **62**, 3683-3704.

Morrison, H., G. Thompson, and V. Tatarskii, 2009: Impact of cloud microphysics on the development of trailing stratiform precipitation in a simulated squall line: Comparison of one- and two-moment schemes. *Mon. Wea. Rev.*, **137**, 991-1007.

Mullendore, G. L., D. R. Durran, and J. R. Holton, 2005: Cross-tropopause tracer transport in midlatitude convection. *J. Geophys. Res.*, **110**, D06113, doi:10.1029/2004JD005059.

Mullendore, G. L., A. J. Homann, K. Bevers, and C. Schumacher, 2009: Radar reflectivity as a proxy for convective mass transport. *J. Geophys. Res.*, **114**, D16103, doi:10.1029/2008JD011431.

Mullendore, G. L., A. J. Homann, S. T. Jorgenson, T. J. Lang, and S. A. Tessendorf, 2013. Relationship between level of neutral buoyancy and dual-Doppler observed mass detrainment levels in deep convection. *Atmos. Chem. Phys.*, **13**, 181-190.

Nordeng, T. E., 1994: Extended versions of the convective parameterization scheme at ECMWF and their impact on the mean and transient activity of the model in the tropics. *Tech. Rep.* **206**, ECMWF.

Olofsson, M.: Global vertical mass transport by clouds- A two-dimensional model study. *Rep. CM-74*, Int. Meteorol. Inst., Stockholm, Sweden, 1988.

Park, R. J., G. L. Stenchikov, K. E. Pickering, R. R. Dickerson, D. J. Allen, and S. Kondragunta, 2001: Regional air pollution and its radiative forcing: Studies with a single-column chemical and radiation transport model. *J. Geophys. Res.*, **106**, 28,751-28,770.

Parker, M. D., and R. H. Johnson, 2000: Organizational modes of midlatitudemesoscale convective systems. *Mon. Wea. Rev.*, **128**, 3413-3436.

Pickering, K. E., A. M. Thompson, J. R. Scala, W. -K. Tao, R. R. Dickerson, and J. Simpson, 1992: Free tropospheric ozone production following entrainment of urban plumes into deep convection. *J. Geophys. Res.*, **97**, 17,985-18,000.

Poulida, O., R. R. Dickerson, and A. Heymsfield, 1996: Stratosphere-troposphere exchange in a midlatitudemesoscale convective complex 1. Observations.*J. Geophys. Res.*, **101**, 6823-6836.

Scala, J. R., and Coauthors, 1990: Cloud draft structure and trace gas transport. *J. Geophys. Res.*, **95**, 17,015-17,030.

Schoen, J. M., and W. S. Ashley, 2011: A climatology of fatal convective wind events by storm type. *Wea. Forecasting*, **26**, 109-121.

Sigmond, M., J. Meloen, and P. C. Siegmund, 2000: Stratosphere-troposphere exchange in an extratropical cyclone, calculated with a Lagrangian method. *Ann. Geophysicae*, **18**, 573-582.

Skamarock, W. C., 2004: Evaluating mesoscale NWP models using kinetic energy spectra. *Mon. Wea. Rev.*, **132**, 3019-3032.

Skamarock, W. C. and Coauthors, 2000: Numerical simulations of the July 10 Stratospheric-Tropospheric Experiment: Radiation, Aerosols, and Ozone/Deep Convection Experiment convective system-Kinematics and transport. *J. Geophys. Res.*, **105**, 19,973-19,990.

Skamarock, W.C., and Coauthors, 2008: A description of the Advanced Research WRF version 3. NCAR Tech. Note NCAR/TN-475+STR, 113 pp.

Stenchikov, G., and Coauthors, 1996: Stratosphere-troposphere exchange in a midlatitude mesoscale convective complex 2. Numerical simulations. *J. Geophys. Res.*, **101**, 6837-6851.

Stoelinga, M. T., cited 2013: A users' guide to RIP version 4.5: A program for visualizing mesoscale model output. [Available online at http://www.mmm.ucar.edu/wrf/users/docs/ripug.htm].

Sukoriansky, S., B. Galperin, and V. Perov, 2006: A quasi-normal scale elimination model of turbulence and its application to stably stratified flows. *Nonlin. Proces. Geophys.*, **13**, 9-22.

Thompson, A. M., and Coauthors, 1994: Convective transport over the central United States and its role in regional CO and ozone budgets. *J. Geophys. Res.*, **99**, 18,703-18,711.

Thompson, A. M., W. –K. Tao, K. E. Pickering, J. R. Scala, and J. Simpson, 1997: Tropical deep convection and ozone formation. *Bull. Amer. Meteor. Soc.*, **78**, 1043-1054.

Thompson, G, R. M. Rasmussen, and K. Manning, 2004: Explicit forecasts of winter precipitation using an improved bulk microphysics scheme. Part I: Description and sensitivity analysis. *Mon. Wea. Rev.*, **132**, 519-542.

Tiedtke, M., 1989: A comprehensive mass flux scheme for cumulus parameterization in large-scale models. *Mon. Wea. Rev.*, **117**, 1779-1800.

Tost, H., P. Jöckel, and J. Lelieveld, 2006b: Influence of different convection parameterisations in a GCM. *Atmos. Chem. Phys*, **6**, 5475-5493.

Tost, H., M. G. Lawrence, C. Brühl, P. Jöckel, The GABRIEL Team, and The SCOUT-O3-DARWIN/ACTIVE Team, 2010: Uncertainties in atmospheric chemistry modelling due to convection parameterisations and subsequent scavenging. *Atmos. Chem. Phys.*, **10**, 1931-1951.

Trier, S. B., F. Chen, and K. W. Manning, 2004: A study of convection initiation in a mesoscale model using high-resolution land surface initial conditions. *Mon. Wea. Rev.*, **132**, 2954-2976.

Vasiloff, S. V., E. A. Brandes, R. P. Davies-Jones, and P. S. Ray, 1986: An investigation into the transition from multicell to supercell storms. *J. Climate Appl. Meteor.*, **25**, 1022-1036.

Weisman, M. L., and J. B. Klemp, 1986: Characteristics of isolated convective storms. *Mesoscale Meteorology and Forecasting*, P. S. Ray, Ed., Amer. Meteor. Soc., 331-358.

Weisman, M. L., W. C. Skamarock, and J. B. Klemp, 1997: The resolution dependence of explicitly modeled convective systems. *Mon. Wea. Rev.*, **125**, 527-548.

Weisman, M. L., C. Davis, W. Wang, K. W. Manning, and J. B. Klemp, 2008: Experiences with 0-36-h explicit convective forecasts with the WRF-ARW model. *Wea. Forecasting*, **23**, 407-437.

Wilcox, E. M., 2003: Spatial and temporal scales of precipitation tropical cloud systems in satellite imagery and the NCAR CCM3. *J. Climate*, **16**, 3545-3559.

Wilhelmson, R. B., and L. J. Wicker, 2001: Numerical modeling of severe local storms. *Severe Convective Storms, Meteor.Monogr.*, No. 50, Amer. Meteor. Soc., 123-166.

World Meteorological Organization (WMO), 1957: Meteorology- a three-dimensional science. *Second session of the Commission for Aerology*.

Wu, J., A. D. Del Genio, M.-S. Yao, and A. B. Wolf, 2009: WRF and GISS SCM simulations of convective updraft properties during TWP-ICE. *J. Geophys. Res.*, **114**, D04206, doi:10.1029/2008JD010851.

Xu, Kuan-Man, and David A. Randall, 2001: Updraft and Downdraft Statistics of Simulated Tropical and Midlatitude Cumulus Convection. *J. Atmos. Sci.*, **58**, 1630–1649.

Zhang, G. J., and N. A. McFarlane, 1995: Sensitivity of climate simulations to the parameterization of cumulus convection in the Canadian Climate Centre Genteral Circulation Model. *Atmos.-Ocean*, **33**, 407-446.

Zhang, Guang J., and Xiaoqing Wu, 2003: Convective Momentum Transport and Perturbation Pressure Field from a Cloud-Resolving Model Simulation.*J. Atmos. Sci.*, **60**, 1120–1139.

Zhang, K., H. Wan, M. Zhang, and B. Wang, 2008: Evaluation of the atmospheric transport in a GCM using radon measurements: sensitivity to cumulus convection parameterization. *Atmos. Chem. Phys.*, **8**, 2811-2832.

Zipser, E. J., and M. A. LeMone, 1980: Cumulonimbus vertical velocity events in GATE. Part II: Synthesis and model core structure. *J. Atmos. Sci.*, **37**, 2458-2469.